INSTITUTO SUPERIOR TÉCNICO
Universidade Técnica de Lisboa

Acoustic Black Holes and Superresonance Mechanisms

Miguel Ereira Mendes Marques

Dissertação para a obtenção de Grau de Mestre em

Engenharia Física Tecnológica

Júri

Presidente: Prof. Dr. José Pizarro de Sande e Lemos
Orientador: Prof. Dr. Vitor Manuel dos Santos Cardoso
Vogal: Prof. Dr. Alfredo Barbosa Henriques

Maio 2011

Acknowledgements

First of all, I would like to thank my supervisor Vitor Cardoso, for all the guidance, patience and support given during my studies. I feel that I've learned a lot with him about the ups and downs of scientific research, and I'm most grateful for this opportunity of working with him.

I'm very thankful to Jorge Rocha, Helvi Witek, Andrea Nerozzi, Térance Delsate, João Mateus, Madalena Lemos, André Moita, Sayan Chakrabarti and Paolo Pani, for very interesting and stimulating group meetings, where I've learned a lot about physics and gravitation.

Last, but surely not least, I want to thank my parents, my brother and Julieta, for all the unconditional support I've always received.

Resumo

Neste trabalho, estudámos um modelo análogo de gravitação, conhecido como buraco negro acústico, baseado na propagação de som em fluidos supersónicos. Demonstramos que, aplicando determinados constrangimentos ao sistema, existe uma correspondência matemática entre mecânica de fluidos e uma variedade lorentziana em relatividade geral. Estendemos o conceito usual da analogia de buracos negros com rotação para o caso do fluido com densidade não constante. Estudamos a geodesia do movimento de campos escalares sem massa no espaço-tempo análogo que consideramos, e encontramos a secção eficaz de absorção válida no limite das altas frequências. Demonstramos a existência do mecanismo de superradiância nestes sistemas acústicos, e calculamos numericamente a amplitude de reflexão de uma onda monocromática. Calculamos numericamente a secção eficaz de absorção, encontrando uma excelente concordância com o resultado analítico obtido para o limite das altas frequências. Finalmente, argumentamos que deverá ser difícil implementar um processo tipo fissão em laboratório.

Palavras-chave: Relatividade Geral, análogos de gravitação, buracos negros, superradiância, buracos acústicos

Abstract

In this work we study an analogue model of gravity, referred to as acoustic black hole, which is based on the propagation of sound waves in supersonic fluids. We show that, considering certain constraints, there is a mathematical correspondence between fluid dynamics and a general relativistic lorentzian manifold. We extend the usual analogy of the rotating black hole to the case of a fluid with non-constant density. We study the geodesy of the motion of massless scalar fields around the considered analogue space-time, and find the absorption cross-section of the acoustic event horizon in the high frequency limit. We show the existence of superradiance in these analogues, and compute numerically the reflected amplitude of the scatter of a monochromatic wave. We compute numerically the absorption cross-section, finding an excellent agreement with the analytical result in the high frequency limit. Finally, we argue that it may be difficult to implement a fission-like process in the laboratory.

Keywords: General relativity, analogue gravity, black holes, superradiance, acoustic holes

This work was supported by Fundação para a Ciência e Tecnologia, under the grant PTDC/FIS/64175/2006. The research included in this thesis was carried out at Centro Multidisciplinar de Astrofísica (CENTRA) in the Physics Department of Instituto Superior Técnico. In the process of this work, one paper has been published - Vitor Cardoso, Madalena Lemos and Miguel Marques, *Instability of Reissner-Nordstrőm black holes in de Sitter backgrounds*, Physical Review D 80, 127502, arXiv: 1001.0019 (2009). Some contents of this thesis are part of original work in progress by Miguel Marques and Vitor Cardoso. The original work in this thesis has been presented in two conferences, namely, - International Conference of Physics Students, Graz, Austria, 17-23 August 2010, and - III Black Holes Workshop, Braga, Portugal, 20-21 December 2010.

Contents

List of Tables

List of Figures

Chapter 1

Introduction

Black holes have been at the center stage of fundamental physics in the last decades: supermassive, astrophysical black holes lurk at the center of most galaxies while large numbers of stellar-mass black holes are thought to populate each galaxy; highly dynamical black hole binaries are strong sources of gravitational waves and, perhaps, power jets and other extreme phenomena. In high-energy physics, black holes are a central piece of the gauge-gravity duality, and are the generic outcome of particle collisions at center-of-mass energies above the Planck scale.

One of the great achievements of quantum field theory in curved backgrounds is Hawking's 1974 semi-classical prediction of black hole evaporation [7]. This process is made possible by the very special nature of the vacuum in quantum field theory, but it is extremely feeble by all astrophysical standards. It is also specific to curved spacetimes with a very special property: the existence of an event horizon. In this "pair-production"-like process, one of the virtual particles falls inside the horizon while the other is radiated away from the black hole, becoming a real particle. In the process, the black hole area will decrease. The need for experimental evidence of Hawking radiation cannot be overstated, as it would confirm this semi-classical phenomenon which perhaps holds some key to a theory of quantum gravity. Unfortunately, for an astrophysical black hole with, say, one solar mass, the time needed for a black hole to evaporate would be of the order of 10^{67} years (the age of the universe is $\sim 10^{10}$ years). The temperature of this radiation would be $\sim 10^{-7}\ K$, much colder than the Cosmic Microwave Background temperature, making it next to impossible to measure Hawking radiation from stellar-like astrophysical black holes.

In 1981, during a lecture on fluid mechanics, Unruh realized that there is a close analogy between a sound wave crossing a supersonic fluid and a light wave crossing an event horizon of a black hole; Unruh went on to establish a mathematically rigorous correspondence between both systems, when the fluid obeys certain conditions [1]. These acoustic analogs, termed as acoustic black holes (or dumb holes, or also sonic holes), do not obey Einstein equations, but they do emit Hawking radiation, and also display the same features of any General Relativity effect which is a consequence of background curvature. Acoustic black holes are a powerful tool providing us the possibility to test experimentally Hawking radiation, as well as any effect happening in the background space-time of a black hole. This analogy as later been "rediscovered" by Visser [8] in 1993, leading to a generalization of the concept to be applied to any general relativistic geometry, and the concept has later been used to create an analogue model of inflationary scenarios in cosmology [9] (more references for this models and other proposed analogue gravity models can be found in Ref. [10]). It was after Visser's revision [2] of the acoustic black hole analogy that the field of the analogue gravity become established on a firm ground, and in the last decade this field has become a mature and important field within the gravity research community. This was not the first time that an analogy with general relativity was thought of. In fact, it was in 1923, shortly after Einstein published his work introducing general relativity, that W. Gordon proposed a description of light propagating in a moving dielectric medium by means of an effective space-time [28](and references there in). Decades later, in 2000, based in this description, Leonhardt et al proposed an optical analogy for black holes.

Besides an event horizon, rotating black holes also display ergoregions, a region in space where particles are forced to co-rotate with the black hole (as seen by observers at infinity), and where they can have negative

energies. Since negative energy states are allowed, a Hawking-like process should also take place. In fact, in 1969, Penrose showed that it is possible to extract energy from a rotating black hole, by having a particle exploding in two within the ergoregion. If one of these two fragments falls into the horizon, then it is possible that the second fragment emerges at infinity with an energy larger than the initial energy of the particle. This is called the Penrose process [5, 6]. This process has a wave analogue, proposed by Zel'dovich in 1971, known as superradiance [13]. The superradiant mechanism is not exclusive of black holes. In this mechanism, a bosonic wave can be reflected out of the black hole with an amplitude higher than the incident wave. There is an instability associated with this mechanism, proposed in 1972 by Press and Teukolsky [27], coined the "black hole fission". They considered a system with many black holes at a close enough distance. The general idea is that a first wave would enter in the ergosphere of one of these black holes, get superradiantly amplified and scatter off another black hole, *ad infinitum*, extracting energy from the system exponentially with time, just as nuclear fission. Press and Teukolsky [26] showed however that such a process could not materialize in realistic astrophysical black hole systems, due to size constraints (the system would be forced to be contained in its own Schwarzschild radius). But these instabilities can in principle be explored in a laboratory, considering that the acoustic black hole is a solution of the Euler equation, rather than a solution of the Einstein equations.

1.1 State of the Art

Several theoretical proposals for experimental models of analogue black holes have been proposed in the last decade [10, 15, 16, 17, 18, 19, 20]. Among them are models based in Bose-Einstein condensates, in plasmas, in water (shalow water waves), in optical fibers and wave-guides, in ion rings, in a superconducting transmission line, etc. In principle, any of this models can be used to exhibit superradiance of phonons. In July 2009, an experimental analogue of a black hole in a Bose-Einstein condensate as been reported in Ref. [14]. In this experiment, Hawking radiation has not been seen mainly because of turbulence caused by making the fluid go supersonic. A way to overcome this problem in the Bose-Einstein condensate experiments has been proposed in Ref. [24] by analyzing the back-reaction. Also, a numerical investigation of hawking radiation arising from Bose-Einstein condensates was realized in Ref. [25]. In August 2010, Weinfurtner et al have reported the observation of stimulated hawking radiation in a shallow water waves experiment [11]. In September 2010, Belgiorno et al reported in the observation of hawking radiation from a spontaneous process in a moving refractive index perturbation experiment in a dielectric medium [12].

Superradiance in acoustic black holes has been studied in [3], and a study of the phenomenon for BEC's has been done in [21]. Quasi-normal modes in acoustic black holes and the "acoustic black hole bomb" instability have been studied in [3, 4]. Also, instabilities in Hawking radiation, similar to those for superradiance studied in this thesis, have been studied in Refs. [22, 23].

1.2 Outline of this thesis

The propose of this thesis is to study the possibility to induce instabilities from superradiance in acoustic black holes. This investigation is useful for a number of reasons, among them it allows one to understand how to explore superradiant effects in the laboratory, or even understand which geometries give rise to larger effects (and perhaps understand also why the Kerr family of black hole solutions has such a low superradiant amplification for most boson fields).

Chapter 2 is intended as an introduction to explain the acoustic analogy of black holes: it begins with a brief review of the fluid dynamics needed to this problem, and the solution of an acoustic wave moving in a (constrained) fluid; then the analogy between this solution and a general relativistic solution for the movement of a scalar field is given, and those solutions are particularized to the case of (2+1) rotating solutions.

Chapter 3 explores the geometry of the above acoustics, deriving the geodesic equations for the particular solution.

Chapter 4 explores the acoustic superradiance ("superresonance") and its instabilities, and numerical solutions of the problem are given.

Finally, in chapter 5 I conclude and also briefly expand on future perspectives and extensions of this work.

In the appendix A I give a full derivation of the Klein-Gordon wave equation considering a fluid with constant density.

Chapter 2

The Acoustic Black Hole Analogy

In this chapter we give a brief, but hopefully self-contained description of how to derive a *"space-time" like* metric out of fluid equations, and then we will find a solution for the case of a geometry allowing rotation of the fluid.

2.1 Fluid Dynamics

Let's start by considering an inviscid, barotropic and locally irrotational fluid, submitted to pressure and gravity forces, and a possible externally imposed driving force. We then have

$$\vec{F} = -\nabla p - \rho\nabla\phi - \rho\nabla\Phi\,, \tag{2.1}$$

were ϕ is the gravitational potential and Φ the potential of the external driving force. Euler equation yields

$$\rho[\partial_t\vec{v} + (\vec{v}\cdot\nabla)\vec{v}] = -\nabla p - \rho\nabla\phi - \rho\nabla\Phi \Leftrightarrow -\frac{1}{\rho}\nabla p - \nabla\phi - \nabla\Phi - (\vec{v}\cdot\nabla)\vec{v} = \partial_t\vec{v}\,, \tag{2.2}$$

and substituting the identity $\frac{1}{2}\nabla v^2 = (\vec{v}\cdot\nabla)\vec{v} + \vec{v}\times(\nabla\times\vec{v})$ in (2.2) we obtain

$$\partial_t\vec{v} = \vec{v}\times(\nabla\times\vec{v}) - \frac{1}{\rho}\nabla p - \nabla(\frac{1}{2}v^2 + \phi + \Phi)\,. \tag{2.3}$$

Because the fluid is locally irrotational (so that the fluid will be vorticity free), we can consider a velocity potential, defined as $\vec{v} = -\nabla\psi$. Considering the fluid to be isentropic, and considering the first law of thermodynamics $dh = Tds + \frac{dp}{\rho}$, where $h = u + \frac{p}{\rho}$ is the specific entalpy and u the internal energy, it follows that $\nabla h = \frac{1}{\rho}\nabla p$. Replacing this result in (2.3) we obtain

$$-\partial_t\nabla\psi = \nabla\psi\times(\nabla\times\nabla\psi) - \nabla h - \nabla(\frac{1}{2}(\nabla\psi)^2 + \phi + \Phi)\,, \tag{2.4}$$

which integrated over the volume results in

$$\Leftrightarrow -\partial_t\psi + h + \frac{1}{2}(\nabla\psi)^2 + \phi + \Phi = 0\,, \tag{2.5}$$

which is a Bernoulli like equation.

2.2 Getting Acoustics into the Fluid

Let us now consider acoustic waves, perturbations in the density ρ, in the pressure p and in the velocity $\vec{v}$ of the fluid, so that we have

$$\rho = \rho_0 + \epsilon\rho_1 + O(\epsilon^2)\,,\quad p = p_0 + \epsilon p_1 + O(\epsilon^2)\,,\quad \vec{v} = \vec{v}_0 + \epsilon\vec{v}_1 + O(\epsilon^2)\,. \tag{2.6}$$

The linearized approximation to the acoustic perturbations is valid for sufficiently low frequencies. The continuity equation will follow as

$$\begin{aligned}
&\partial_t \rho + \nabla \cdot (\rho \vec{v}) = 0\,, \\
&\Leftrightarrow \partial_t(\rho_0 + \epsilon\rho_1) + \nabla \cdot ((\rho_0 + \epsilon\rho_1)(\vec{v}_0 + \epsilon\vec{v}_1)) = 0\,, \\
&\Leftrightarrow \partial_t\rho_0 + \epsilon\partial_t\rho_1 + \nabla \cdot (\rho_0\vec{v}_0 + \rho_0\epsilon\vec{v}_1 + \epsilon\rho_1\vec{v}_0 + \epsilon^2\rho_1\vec{v}_1) = 0\,,
\end{aligned} \tag{2.7}$$

and discarding the terms with ϵ^2, one can clearly separate this result in two equations

$$\partial_t\rho_0 + \nabla \cdot (\rho_0\vec{v}_0) = 0\,, \tag{2.8}$$

and

$$\partial_t\rho_1 + \nabla \cdot (\rho_1\vec{v}_0 + \rho_0\vec{v}_1) = 0\,. \tag{2.9}$$

It is easy to understand that being the velocity perturbed, by its definition the velocity potencial ψ will also be perturbed, becoming $\psi = \psi_0 + \epsilon\psi_1 + O(\epsilon^2)$. The Taylor expansion of the specific enthalpy in the neighbourhood of p_0 will result in

$$\begin{aligned}
h &= h_0 + \left(\frac{dh}{dp}\right)_{p=p_0}(p - p_0) + O(\epsilon^2) = h_0 + \frac{1}{\rho_0}(p - p_0) + O(\epsilon^2)\,, \\
&= h_0 + \epsilon\frac{p_1}{\rho_0} + O(\epsilon^2)\,,
\end{aligned} \tag{2.10}$$

then, equation (2.5) becomes

$$-\partial_t(\psi_0 + \epsilon\psi_1) + h_0 + \epsilon\frac{p_1}{\rho_0} + \frac{1}{2}(\nabla(\psi_0 + \epsilon\psi_1))^2 + \phi + \Phi = 0\,, \tag{2.11}$$

and discarding the terms with ϵ^2, one obtains the equations

$$-\partial_t\psi_0 + h_0 + \frac{1}{2}(\nabla\psi_0)^2 + \phi + \Phi = 0\,, \tag{2.12}$$

and

$$\begin{aligned}
&-\epsilon\partial_t\psi_1 + \epsilon\frac{p_1}{\rho_0} + \frac{1}{2}2\nabla\psi_0\epsilon\nabla\psi_1 = 0 \Leftrightarrow -\partial_t\psi_1 + \frac{p_1}{\rho_0} + \nabla\psi_0\nabla\psi_1 = 0 \Leftrightarrow -\partial_t\psi_1 + \frac{p_1}{\rho_0} - \vec{v}_0 \cdot \nabla\psi_1 = 0 \\
&\Leftrightarrow p_1 = \rho_0(\partial_t\psi_1 + \vec{v}_0 \cdot \nabla\psi_1)\,.
\end{aligned} \tag{2.13}$$

Because the fluid is taken to be barotropic, we shall consider a Taylor expansion of the density ρ in the neighborhood of the pressure p_0, so that we have

$$\rho(p) = \rho_0 + \epsilon\rho_1 + O(\epsilon^2) = \rho(p_0) + \left(\frac{d\rho}{dp}\right)_{p=p_0}(p - p_0) + O(p^2)\,. \tag{2.14}$$

This yields

$$\rho_1 = \frac{\partial\rho}{\partial p}p_1 = \frac{\partial\rho}{\partial p}\rho_0(\partial_t\psi_1 + \vec{v}_0 \cdot \nabla\psi_1)\,. \tag{2.15}$$

Replacing (2.15) in (2.9), we have

$$\begin{aligned}
&\partial_t\left(\frac{\partial\rho}{\partial p}\rho_0(\partial_t\psi_1 + \vec{v}_0 \cdot \nabla\psi_1)\right) + \nabla \cdot \left(\left(\frac{\partial\rho}{\partial p}\rho_0(\partial_t\psi_1 + \vec{v}_0 \cdot \nabla\psi_1)\right)\vec{v}_0 + \rho_0\vec{v}_1\right) = 0\,, \\
&\Leftrightarrow \partial_t\left(\frac{\partial\rho}{\partial p}\rho_0(\partial_t\psi_1 + \vec{v}_0 \cdot \nabla\psi_1)\right) + \nabla \cdot \left(\left(\frac{\partial\rho}{\partial p}\rho_0\vec{v}_0(\partial_t\psi_1 + \vec{v}_0 \cdot \nabla\psi_1)\right) - \rho_0\nabla\psi_1\right) = 0\,, \\
&\Leftrightarrow -\partial_t\left(\frac{\partial\rho}{\partial p}\rho_0(\partial_t\psi_1 + \vec{v}_0 \cdot \nabla\psi_1)\right) + \nabla \cdot \left(\left(-\frac{\partial\rho}{\partial p}\rho_0\vec{v}_0(\partial_t\psi_1 + \vec{v}_0 \cdot \nabla\psi_1)\right) + \rho_0\nabla\psi_1\right) = 0\,.
\end{aligned} \tag{2.16}$$

Knowing that the speed of a sound wave is $c = \sqrt{\frac{dp}{d\rho}}$, we can rewrite (2.16) as

$$-\partial_t(\frac{\rho_0}{c^2}(\partial_t\psi_1+\vec{v}_0\cdot\nabla\psi_1))+\nabla\cdot(\rho_0\nabla\psi_1-\frac{\rho_0}{c^2}\vec{v}_0(\partial_t\psi_1+\vec{v}_0\cdot\nabla\psi_1))=0$$

$$\Leftrightarrow -\frac{\rho_0}{c^2}\partial_t(\partial_t\psi_1+\vec{v}_0\cdot\nabla\psi_1)+\frac{\rho_0}{c^2}\nabla\cdot(c^2\nabla\psi_1-\vec{v}_0(\partial_t\psi_1+\vec{v}_0\cdot\nabla\psi_1))=0. \tag{2.17}$$

It is now convenient to reformulate equation (2.17) in a tensorial form. Following (2.17), one can construct a matrix $f^{\mu\nu}(t,\vec{x})$ as

$$f^{\mu\nu}(t,\vec{x})=\frac{\rho_0}{c^2}\begin{pmatrix} -1 & -v_0^{x_1} & -v_0^{x_2} & -v_0^{x_3} \\ -v_0^{x_1} & c^2-v_0^{x_1}v_0^{x_1} & -v_0^{x_1}v_0^{x_2} & -v_0^{x_1}v_0^{x_3} \\ -v_0^{x_2} & -v_0^{x_2}v_0^{x_1} & c^2-v_0^{x_2}v_0^{x_2} & -v_0^{x_2}v_0^{x_3} \\ -v_0^{x_3} & -v_0^{x_3}v_0^{x_1} & -v_0^{x_3}v_0^{x_2} & c^2-v_0^{x_3}v_0^{x_3} \end{pmatrix}, \tag{2.18}$$

so that (2.17) becomes

$$\partial_\mu(f^{\mu\nu}\partial_\nu\psi_1)=0\,. \tag{2.19}$$

2.3 The Acoustic Metric

The Klein-Gordon equation for a minimally coupled massless scalar field follows as

$$\frac{1}{\sqrt{-g}}\partial_\mu(\sqrt{-g}g^{\mu\nu}\partial_\nu\psi)=0, \tag{2.20}$$

where g is the determinant of the metric tensor $g_{\mu\nu}$. Comparing equations (2.19) and (2.20), one finds a clear mathematical correspondence. Indeed, considering the relation $f^{\mu\nu}\leftrightarrow\sqrt{-g}g^{\mu\nu}$, one can find a formal correspondence between a scalar field propagating in a curved spacetime with metric $g^{\mu\nu}$ and a sound wave in flat Minkowski spacetime in a certain background flow (which determines the metric of the analog curved spacetime).

The determinant of $f^{\mu\nu}(t,\vec{x})$ is

$$\det(f^{\nu\mu})=\det(\sqrt{-g}g^{\mu\nu})=(\sqrt{-g})^4g^{-1}=g\,, \tag{2.21}$$

and computing the determinant from (2.18) we obtain

$$g=\det(f^{\mu\nu})=-\frac{\rho_0}{c^2}\,. \tag{2.22}$$

Therefore, we have

$$g^{\mu\nu}(t,\vec{x})=\frac{1}{\rho_0 c}\begin{pmatrix} -1 & \vdots & -v_0^j \\ \cdots\cdots\cdots & . & \cdots\cdots\cdots\cdots \\ -v_0^i & \vdots & c^2\delta^{ij}-v_0^iv_0^j \end{pmatrix}, \tag{2.23}$$

Inverting this result, one finally obtains an effective spacetime metric, given by

$$g_{\mu\nu}(t,\vec{x})=\frac{\rho_0}{c}\begin{pmatrix} -(c^2-v_0^2) & \vdots & -v_0^j \\ \cdots\cdots\cdots & . & \cdots\cdots\cdots\cdots \\ -v_0^i & \vdots & \delta^{ij} \end{pmatrix}, \tag{2.24}$$

Equivalently, the line element is

$$ds^2\equiv g_{\mu\nu}dx^\mu dx^\nu=\frac{\rho_0}{c}\left[-c^2dt^2+\left(dx^i-v_0^idt\right)\delta_{ij}\left(dx^j-v_0^jdt\right)\right]. \tag{2.25}$$

2.4 The Vortex Geometry Solution

We now particularize the line element (2.25) to a solution which can be seen as an analogue of the Kerr solution (in the equatorial plane), in which the spacetime is rotating and there is a clear distinction between the ergosphere and the acoustic event horizon. From here onwards we refer to this as the *"draining bathtub"* fluid flow.

Let's consider a (2+1) dimensional *"draining bathtub"* fluid flow with a sink at the origin. From the continuity equation, one finds the radial component of the velocity to be

$$\begin{aligned} &\partial_r \left(\rho r v^{\hat{r}}\right) = 0 \Leftrightarrow \int \partial_r \left(\rho r v^{\hat{r}}\right) dr = cte\,, \\ &\Leftrightarrow \rho v^{\hat{r}} = \frac{cte}{r}\,. \end{aligned} \tag{2.26}$$

Since the fluid is taken to be irrotational, the angular component of the velocity is

$$\begin{aligned} &\nabla \times \vec{v} = \frac{1}{r}\left(\partial_r \left(r v^{\hat{\theta}}\right) - \partial_\theta v^{\hat{r}}\right) = \frac{1}{r}\partial_r \left(r v^{\hat{\theta}}\right) = 0\,, \\ &\Leftrightarrow v^{\hat{\theta}} = \frac{cte}{r}\,. \end{aligned} \tag{2.27}$$

The angular momentum of the fluid will be $L = \rho V r v^{\hat{\theta}}$ (were V is the volume of the *draining bathtub*, taken to be constant). Now, the irrotational condition gives us that

$$\begin{aligned} &\frac{1}{r}\partial_r \left(r v^{\hat{\theta}}\right) = \frac{1}{r}\partial_r \left(\frac{L}{\rho V}\right) = 0\,, \\ &\Leftrightarrow \frac{L}{\rho} = cte\,, \end{aligned} \tag{2.28}$$

therefore, if we assume the conservation of the angular momentum, the background density ρ must also be constant. The velocity potential is

$$\begin{aligned} &\nabla\psi = \left(\partial_r \psi_r, \frac{1}{r}\partial_\theta \psi_\theta\right) = -\vec{v} = \left(-\frac{A}{r}, -\frac{B}{r}\right)\,, \\ &\Leftrightarrow \psi(r,\theta) = -A \ln r - B\theta\,. \end{aligned} \tag{2.29}$$

The velocity of the background flow is

$$\vec{v} = \frac{A\hat{r} + B\hat{\theta}}{r}. \tag{2.30}$$

Replacing (2.30) in the line element (2.25), considering $\rho_0 = c$ with c being a constant speed, we obtain

$$\begin{aligned} ds^2 &= -c^2 dt^2 + \left(dr - \frac{A}{r}dt\right)^2 + \left(r d\theta - \frac{B}{r}dt\right)^2 = \\ &= -\left(c^2 - \frac{A^2 + B^2}{r^2}\right) dt^2 - 2\frac{A}{r} dr dt - 2B d\theta dt + dr^2 + r^2 d\theta^2. \end{aligned} \tag{2.31}$$

Applying the following coordinate transformation (written as in Ref. [3])

$$dt \to d\tilde{t} + \frac{Ar}{r^2c^2 - A^2}dr, \qquad d\theta \to d\tilde{\theta} + \frac{BA}{r\left(r^2c^2 - A^2\right)}dr, \tag{2.32}$$

one forces the line element to be written in a Kerr-like form,

$$ds^2 = -\left(1 - \frac{A^2 + B^2}{c^2 r^2}\right) c^2 d\tilde{t}^2 + \left(1 - \frac{A^2}{c^2 r^2}\right)^{-1} dr^2 - 2B d\tilde{\theta} d\tilde{t} + r^2 d\tilde{\theta}^2. \tag{2.33}$$

The effective geometry (2.33) has an event horizon at

$$r_H = \frac{|A|}{c}, \tag{2.34}$$

and the ergoregion, defined as the locus of $d\tilde{t}^2 = 0$ is delimited by the boundary

$$r_{ergo} = \frac{\sqrt{A^2 + B^2}}{c}. \tag{2.35}$$

2.5 Generalizing the Rotating Geometry

In 2.4 we have considered a case of a fluid with constant density and a constant speed of sound. This is the case found in the typical literature [2, 3]. In section 4.2 it will be useful to have a geometry with a non constant density. Considering the line element (2.25) for a (2+1) rotating geometry we have

$$ds^2 = \frac{\rho}{c}\left[-c^2dt^2 + (dr - v^r dt)^2 + \left(rd\theta - v^\theta dt\right)^2\right], \tag{2.36}$$

and applying the following transformations in order to have a Kerr-like form

$$dt \to dt - \frac{v^r}{(c^2 - (v^r)^2)}dr, \qquad d\theta \to d\theta - \frac{v^\theta}{r}\frac{v^r}{(c^2 - (v^r)^2)}dr\,, \tag{2.37}$$

we then have

$$ds^2 = \frac{\rho}{c}\left(\frac{c^2}{c^2 - (v^r)^2}dr^2 + \left(v^2 - c^2\right)dt^2 - 2rv^\theta dtd\theta + r^2d\theta^2\right). \tag{2.38}$$

Now, as before, we will consider $\rho = c$, but with $c = c(r)$ being position dependent. From equation (2.26) we will write $v^r = A'/(c(r)r)$[1], and from equation(2.27) we will write $v^\theta = B/r$. Equation (2.38) becomes

$$ds^2 = \left(\frac{c(r)^2}{c(r)^2 - (v^r)^2}dr^2 + (v^2 - c(r)^2)dt^2 - 2Bdtd\theta + r^2d\theta^2\right), \tag{2.39}$$

which can be rewritten as

$$ds^2 = -\left(c(r)^2 f(r) - \left(\frac{B}{r}\right)^2\right)dt^2 + \frac{1}{f(r)}dr^2 - 2Bdtd\theta + r^2d\theta^2, \tag{2.40}$$

where $f(r) = 1 - (v^r)^2/c(r)^2 = 1 - A'^2/c(r)^4r^2$. In chapter 4, it will be very useful to consider some density profile such that there will be some sort of *mass shield* surrounding the acoustic black hole, so that instabilities occur from the superradiance process. We will know introduce such a density profile, by defining, in an *ad-hoc* way, the speed of sound to be given by

$$c(r) = 2 - \frac{1}{r^n}, \tag{2.41}$$

where n will be considered to be a positive integer in the next chapters only for computational purposes, but there is no reason why it can't be any other positive real number. With this density profile, we can't have an analytical result of either the event horizon or the boundary of the ergoregion. However, we find that setting $A = 1$, the solution of the event horizon becomes $r_H = 1$. As for the radius of the ergoregion boundary, we find that as the index n increases, it decreases quickly to

$$r_{ergo} \sim \frac{1}{4}\sqrt{A^2 + 4B^2}\,, \quad n \to \infty\,, \tag{2.42}$$

and for large rotations, we have

$$r_{ergo} \sim \frac{B}{2}\,, \quad B \to \infty\,. \tag{2.43}$$

[1]Here, A' is not the same as A in (2.30), as in the later, ρ has been considered a constant and therefore we implicitly wrote $A = A'/\rho$

Chapter 3

Geodesics in The "Draining Bathtub" Metric

In general relativity, the motion of particles in a space-time is described by the geodesic equations. In this chapter, we will study the geodesic equations for a phonon in the analogue space-time. These results will be used later in chapter 4 to compare the numerical cross-section with the analytical cross-section results. Geodesics in general relativity have already been verified by observations in astronomy, however, the present results could allow a further experimental proof for general relativity.

3.1 Null Geodesics I: The Vortex Geometry with constant density

Writing down the Lagrangian for the line element (2.33), we have

$$2\mathcal{L} = -\left(c^2 - \frac{A^2+B^2}{r^2}\right)\dot{t}^2 + \left(1 - \frac{A^2}{c^2 r^2}\right)^{-1}\dot{r}^2 - 2B\dot{\theta}\dot{t} + r^2\dot{\theta}^2, \tag{3.1}$$

where dots stand for derivative with respect to proper time τ.

Since the Lagrangian doesn't depend explicitly on the variables t and θ, one will have the two conserved quantities in $p_t = \frac{\partial \mathcal{L}}{\partial \dot{t}}$ and $p_\theta = \frac{\partial \mathcal{L}}{\partial \dot{\theta}}$, being them

$$p_t = -\left(c^2 - \frac{A^2+B^2}{r^2}\right)\dot{t} - B\dot{\theta} = -\frac{E'}{m} = -E, \tag{3.2}$$

and

$$p_\theta = r^2\dot{\theta} - B\dot{t} = \frac{L'}{m} = L, \tag{3.3}$$

where E' is the phonon energy, L' is the phonon angular momentum and m is the mass of the quantity of fluid which is perturbed by the phonon. For simplicity, the mass term m will be contracted with the energy E' and the angular momentum L', and we will consider the constant quantities E and L. For null geodesics we have

$$2\mathcal{L} = -E\dot{t} + L\dot{\theta} + \left(1 - \frac{A^2}{c^2 r^2}\right)^{-1}\dot{r}^2 = 0. \tag{3.4}$$

Re-writing equation (3.3) as

$$\dot{t} = \frac{1}{B}\left(r^2\dot{\theta} - L\right), \tag{3.5}$$

and using this result in (3.2), we have

$$E = \left(c^2 - \frac{A^2+B^2}{r^2}\right)\frac{1}{B}\left(r^2\dot{\theta} - L\right) + B\dot{\theta}\,. \tag{3.6}$$

Solving the above for $\dot{\theta}$ yields

$$\dot{\theta} = \frac{L\left(c^2 - \frac{A^2+B^2}{r^2}\right) + EB}{r^2c^2 - A^2}\,. \tag{3.7}$$

Replacing (3.7) and (3.5) in (3.4), and solving for $\dot{r}^2$, we get finally

$$\dot{r}^2 = \frac{\left(A^2+B^2\right)L^2 - L\left(2BE + c^2L\right)r^2 + E^2r^4}{c^2r^4}. \tag{3.8}$$

Let us define the impact parameter as

$$D = \frac{L}{E}\,, \tag{3.9}$$

in terms of which our results for the geodesic equations can be written as

$$\dot{r}^2 = L^2\frac{A^2+B^2-\left(\frac{2B}{D}+c^2\right)r^2+\frac{r^4}{D^2}}{c^2r^4}\,, \tag{3.10}$$

$$\dot{\theta} = L\frac{c^2-\frac{A^2+B^2}{r^2}+\frac{B}{D}}{r^2c^2-A^2}\,, \tag{3.11}$$

$$\dot{t} = L\frac{\frac{r^2}{D}-B}{c^2r^2-A^2}\,. \tag{3.12}$$

Considering equation (3.11) for large distances, we get

$$r^2\dot{\theta} = L + \frac{EB}{c^2}, \quad r\to\infty\,, \tag{3.13}$$

which shows that the acoustic hole rotation has influence at infinity. The phonon's total angular momentum is defined by

$$L_{\text{total}} = r^2\dot{\theta} = L + \frac{EB}{c^2}. \tag{3.14}$$

Recalling that the fluid angular momentum is $L_{\text{fluid}} = mrv^{\hat{\theta}}$, which in fact is the second term in (3.14), we see that the total angular momentum is a linear addition of the phonon's angular momentum with the background angular momentum, which is a frame-dragging effect.

Zero Angular Momentum Geodesics

We now consider zero angular momentum geodesic, $L = 0$, the closest to radial motion one can think of in rotating black hole spacetimes. However, we will see that the trajectories are not radial, the particles are "dragged" by inertial forces associated with the rotation of the background spacetime. Furthermore, from equation (3.14) we get that the total angular momentum is $L_{\text{total}} = \frac{EB}{c^2}$, which means that this is not, in reality, a *"zero angular momentum geodesic"* in a rotating acoustic hole. Equations (3.10), (3.11) and (3.12) reduce to, when $L = 0$,

$$\dot{r}^2 = \frac{E^2}{c^2}\,, \tag{3.15}$$

$$\dot{\theta} = \frac{EB}{c^2r^2-A^2}\,, \tag{3.16}$$

$$\dot{t} = E\frac{r^2}{c^2r^2-A^2}\,. \tag{3.17}$$

We can then write the equations of motion of a phonon with zero angular momentum as

$$\frac{dr}{dt} = \pm\left(c - \frac{A^2}{cr^2}\right)\,, \tag{3.18}$$

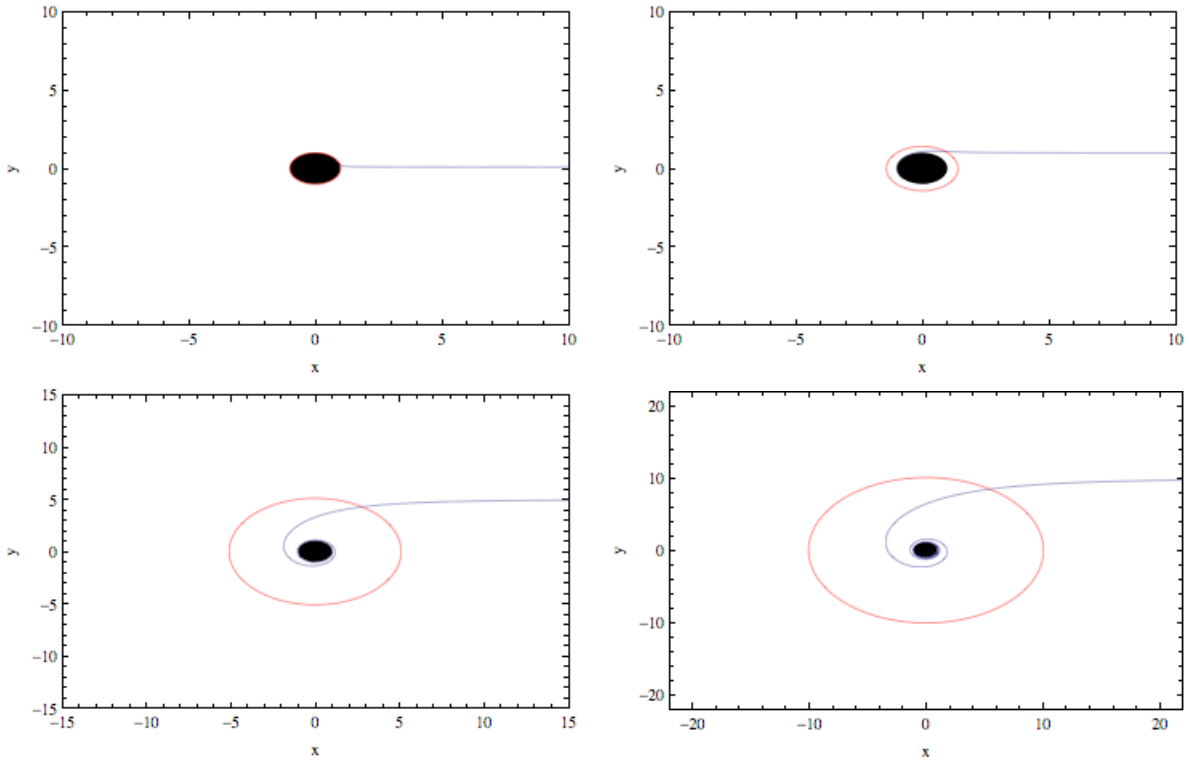

Figure 3.1: Zero angular momentum ($L = 0$) geodesics for $B = 0.1, 1, 5, 10$ (top to bottom, left to right). The red circle represents the ergoregion.

and

$$\frac{d\theta}{dt} = \frac{B}{r^2}\,. \tag{3.19}$$

In figure 3.1, we show geodesics for sound waves coming from the infinity, with an initial angle $\theta = 0$, for $B = 0.1, 1, 5, 10$ (in units such that A=c=E=1). As expected, we see that, when regarding large distances (in respect to the acoustic horizon), we see particles traveling with a finite impact parameter.

As we see, these are not zero-impact parameter trajectories, on account of relation (3.14): these geodesics behave as having an effective angular momentum given by $L_{\text{total}} = \frac{EB}{c^2}$. Thus, the closest one could get to zero-impact parameter geodesics would be to consider an angular momentum of $L = -L_{\text{fluid}} = -\frac{EB}{c^2}$, such that $L_{\text{total}} = 0$.

Null circular geodesics and critical impact parameter

We now want to study the some important geodesics in the spacetime. We begin with null circular geodesics, for which $\dot{r} = \ddot{r} = 0$. The radial acceleration of the phonon can be computed from given by the equation $V_{eff}^2 = E^2 - \dot{r}^2$. We have

$$\ddot{r} = -\frac{1}{2}\frac{d}{dr}V_{eff}^2, \tag{3.20}$$

and therefore,

$$\ddot{r} = L^2\frac{-2\left(A^2+B^2\right) + \left(\frac{2B}{D} + c^2\right)r^2}{c^2 r^5}. \tag{3.21}$$

Solving equations (3.10) and (3.21) for the radius r_c of this circular orbit, we find

$$r_c = \frac{\sqrt{2\left(A^2+B^2 \mp B\sqrt{A^2+B^2}\right)}}{c}\,. \tag{3.22}$$

The upper and lower signs refer to co- and counter-rotating orbits, respectively. For zero rotation ($B = 0$), we find

$$r_c = \frac{\sqrt{2}A}{c} = \sqrt{2}r_H\,, \qquad B = 0\,. \tag{3.23}$$

For very large rotations, we find

$$r_c \sim r_H\,, \quad B \to \infty\,, \qquad \text{co-rotating} \tag{3.24}$$

$$r_c \sim 2B/c \sim 2r_{\text{ergo}}\,, \quad B \to \infty\,, \qquad \text{counter-rotating} \tag{3.25}$$

The angular velocity at each orbit is

$$\frac{d\theta}{dt} = c^2\frac{B \pm \sqrt{A^2 + B^2}}{2A^2}. \tag{3.26}$$

Finally, the impact parameter at the circular null geodesic also coincides with the critical impact parameter for phonon capture and, in units such that $c = 1$, is given by

$$D_c = -2\left(B \mp \sqrt{A^2 + B^2}\right)\,, \tag{3.27}$$

for co- and counter-rotating geodesics respectively. For very large rotations, equation (3.27) yields

$$D_c \sim 0\,, \quad B \to \infty\,, \qquad \text{co-rotating} \tag{3.28}$$

$$D_c \sim -4B \sim -4r_{\text{ergo}}\,, \quad B \to \infty\,, \qquad \text{counter-rotating} \tag{3.29}$$

The reason why, for large rotations, co-rotating waves aren't absorbed, can be understood by observing in equation (3.14) that, in this metric, contrary to what happens in a *Kerr space-time*, the angular velocity of the acoustic hole does have an effect in the infinity, and therefore the total angular momentum one sees when a wave coming from the infinity arrives close to the acoustic hole, is much larger than the angular momentum that the wave initially had. On the other hand, a compensation of this effect happens, for the same reason, with counter-rotating waves , which at large rotations are always absorbed. Figure 3.2 represent the variation of the effective potential with the impact parameter for $B = 3$ and a fixed time. In figure 3.3, we show plots

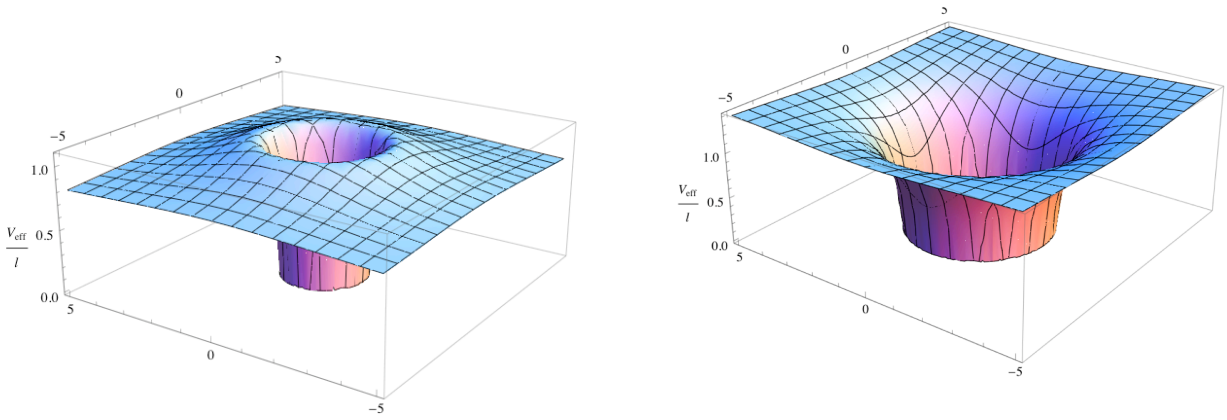

Figure 3.2: Effective potential V_{eff}/L for impact parameter $D = D_c \pm 1$.

for geodesics with several $co-$ and $counter-rotating$ angular momentums.

3.2 Null Geodesics II: The Generalized Rotating Geometry

We now write the lagrangian density for the line element (2.40)

$$2\mathcal{L} = -\left(c^2(r)f(r) - \frac{B^2}{r^2}\right)\dot{t}^2 + \frac{1}{f(r)}\dot{r}^2 - 2B\dot{\theta}\dot{t} + r^2\dot{\theta}^2, \tag{3.30}$$

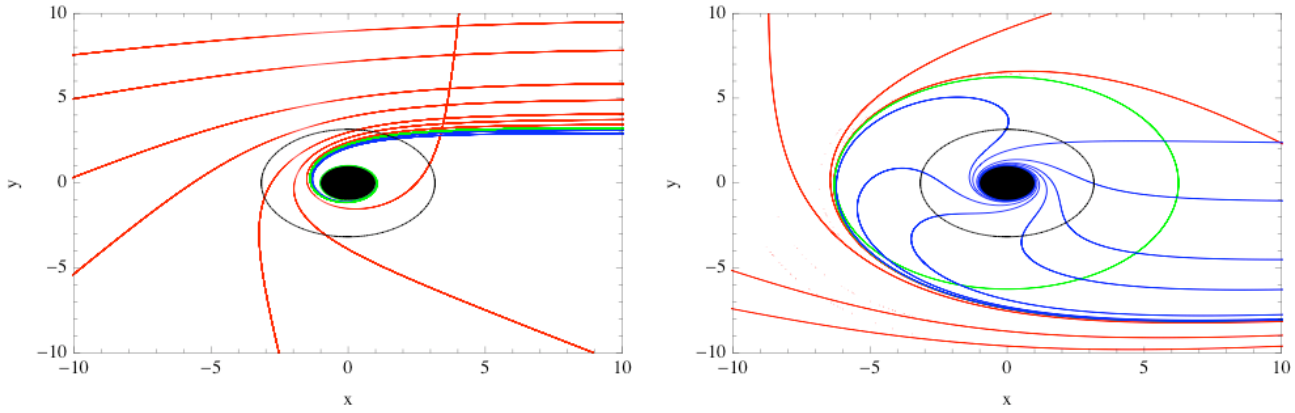

Figure 3.3: Geodesics for co- and counter-rotating waves with $B = 3$, (left and right panel, respectively). Blue lines stand for phonons which fall into the hole, green lines are critical null geodesics and red lines stand for scattered trajectories.

and for null geodesics, we have $\mathcal{L} = 0$. Again, we will have the conserved quantities $p_t = -\frac{E'}{m} = -E$ and $p_\theta = \frac{L'}{m} = L$, which are

$$E = \left(c^2(r)f(r) - \frac{B^2}{r^2}\right)\dot{t} + B\dot{\theta}\,, \tag{3.31}$$

and

$$L = r^2\dot{\theta} - B\dot{t}\,, \tag{3.32}$$

and therefore it follows that

$$-E\dot{t} + L\dot{\theta} + \frac{1}{f(r)}\dot{r}^2 = 0. \tag{3.33}$$

Rewriting (3.32) as (3.5) and replacing in (3.31) we find

$$E = \left(c^2(r)f(r) - \frac{B^2}{r^2}\right)\frac{1}{B}\left(r^2\dot{\theta} - L\right) + B\dot{\theta}\,. \tag{3.34}$$

Finally, we obtain the geodesic equations

$$\dot{r}^2 = L^2\frac{B^2 - \left(\frac{2B}{D} + c^2(r)f(r)\right)r^2 + \frac{r^4}{D^2}}{c^2(r)r^4}\,, \tag{3.35}$$

$$\dot{\theta} = L\frac{\frac{B}{D} + \left(c^2(r)f(r) - \frac{B^2}{r^2}\right)}{c^2(r)r^2f(r)}\,, \tag{3.36}$$

$$\dot{t} = L\frac{\frac{r^2}{D} - B}{c^2(r)r^2f(r)}\,. \tag{3.37}$$

Zero Angular Momentum Geodesics

If the phonon has no angular momentum, $L = 0$, then equations (3.35), (3.36) and (3.37) become

$$\dot{r}^2 = \frac{E^2}{c^2(r)}\,, \tag{3.38}$$

$$\dot{\theta} = \frac{EB}{c^2(r)r^2f(r)}\,, \tag{3.39}$$

$$\dot{t} = \frac{E}{c^2(r)f(r)}\,. \tag{3.40}$$

The equations of motion of a phonon across a radial geodesic is then

$$\frac{dr}{dt} = \pm\left(\frac{c(r)}{f(r)}\right), \tag{3.41}$$

and

$$\frac{d\theta}{dt} = \frac{B}{r^2}. \tag{3.42}$$

Null circular geodesics and critical impact parameter

From equation (3.20), we can compute the radial acceleration of the phonon to be

$$\ddot{r} = L^2 \frac{4BD\left(r^2 - BD\right)c(r) - 2r\left(r^2 - BD\right)^2 \partial_r c(r) + D^2 r^2 c^3(r)\left(2f(r) - r\partial_r f(r)\right)}{2D^2 r^5 c^3(r)}. \tag{3.43}$$

To have circular geodesics, we will impose $\dot{r} = \ddot{r} = 0$. We will know consider that the speed of sound will follow a profile as in 2.41. The results for the radius of null circular orbits and the correspondent critical impact parameters can't be solved analytically for this density profile. Tables 3.1 and 3.2 show numerical results for this orbits, setting $A = 1$ (which will set the event horizon at $r_H = 1$).

	$co-rotating$		$counter-rotating$	
B	r_c	D_c	r_c	D_c
0	1.29147	0.777114	1.29147	-0.777115
1	1.16021	0.509428	1.57606	-1.27827
2	1.09631	0.363065	2.17978	-2.07886
3	1.06331	0.276637	3.06512	-3.03223
4	1.04465	0.221411	4.03468	-4.01936
5	1.03313	0.183695	5.02342	-5.01404
6	1.02552	0.156542	6.01789	-6.01116
7	1.02022	0.136163	7.01461	-7.00933
8	1.01639	0.120356	8.01243	-8.00805
9	1.01353	0.107764	9.01086	-9.00709
10	1.01134	0.097511	10.0097	-10.0063

Table 3.1: Critical radius and critical impact parameter with n=5

We find in table 3.1 that as B increases, co-rotating orbits approach r_H, and the respective impact parameter becomes a very small number, while counter-rotating orbits approach $\sim 2r_{\text{ergo}} \sim B$, and the respective impact parameter approach B. We also find in table 3.2 that the larger the value of the index n is, the smaller is the effect it has on the geodesics. Also, we find that for large values of n, for counter-rotating particles we will have

$$r_c \sim \sqrt{\frac{A^2}{8} + \frac{B^2}{2} + \frac{1}{4}\sqrt{A^2B^2 + 4B^4}}, \quad n \to \infty, \tag{3.44}$$

$$D_c \sim \frac{-2B^2 - \sqrt{B^2\left(A^2 + 4B^2\right)}}{4B}, \quad n \to \infty\,. \tag{3.45}$$

The results for $n = 0$ correspond to the case of constant density, and they match the values we obtain from equations 3.22 and 3.27. In figure 3.4, we show a numerical plot of the evolution of the angular velocity $\frac{d\theta}{dt}$ for a co-rotating particle at the null circular orbit, with the rotation parameter B. We find that, as expected, for large rotations we get $\frac{d\theta}{dt} = B$. As for the case of the constant density, the particles angular momentum will be added the background angular momentum as it propagates in the fluid. For the considered density profile2.41, the total angular momentum the particle will have, when coming from the infinity, is

$$L_{\text{total}} = L + \frac{EB}{4}. \tag{3.46}$$

	$co-rotating$		$counter-rotating$	
n	r_c	D_c	r_c	D_c
0	1.00489	0.198039	10.1484	-20.198
1	1.01372	0.194382	6.02204	-6.01348
2	1.02073	0.191147	5.30225	-5.20294
3	1.02603	0.188325	5.09586	-5.05131
4	1.03004	0.185861	5.03828	-5.02032
5	1.03313	0.183695	5.02342	-5.01404
6	1.03556	0.181774	5.01988	-5.01286
7	1.03749	0.180054	5.01848	-5.01206
8	1.03903	0.178502	5.01861	-5.01243
9	1.04026	0.177093	5.01871	-5.01247
10	1.04123	0.175807	5.01871	-5.01247
11	1.04199	0.174627	5.01871	-5.01247
12	1.04255	0.173540	5.01870	-501247

Table 3.2: Critical radius and critical impact parameter with B=5

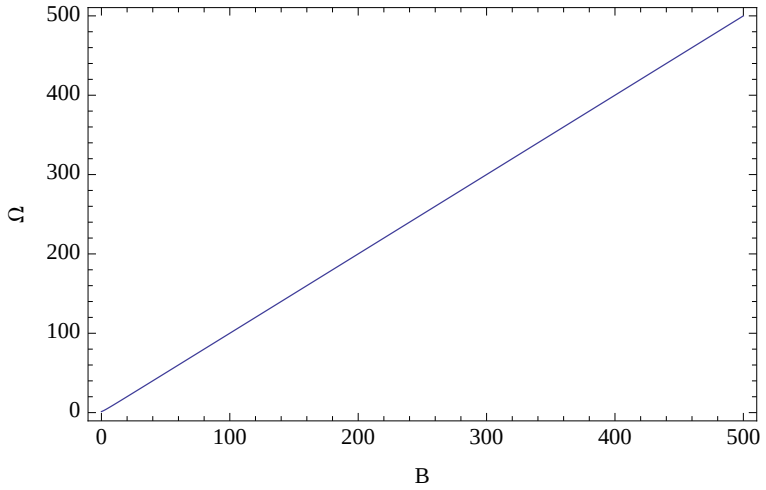

Figure 3.4: Angular velocity of co-rotating particles at the null circular orbit

Note however that, although we defined the impact parameter D as (3.9), to obtain the perpendicular distance between the sound trajectory and to the center of the acoustic hole, one must multiply this parameter by the speed of sound c, and hence, since in this case, for large distances, we have from (2.41) that $c \sim 2$, the impact distance that one will observe in this conditions won't be $\frac{L_{\text{total}}}{E}$ but

$$\frac{2}{E}\left(L + \frac{EB}{4}\right). \tag{3.47}$$

In figure 3.5, we show plots for geodesics with several $co-$ and $counter-rotating$ angular momentums.

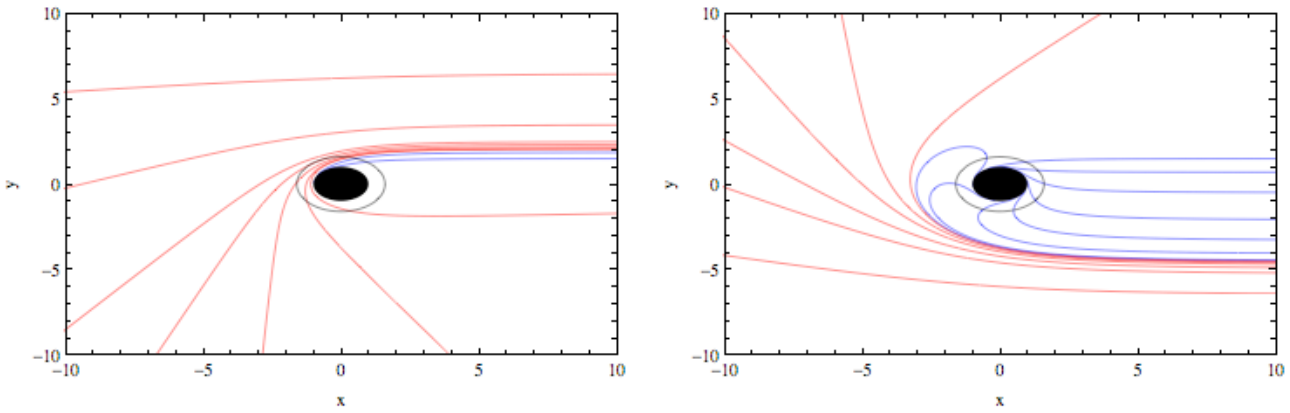

Figure 3.5: Geodesics for co- and counter-rotating waves in a fluid for non-constant density, with $B = 3$, respectively left and right. Blue lines are absorbed geodesics and red lines are scattered geodesics.

Chapter 4

Superresonance in Acoustic Holes

Superradiance is a phenomenon which can occur in systems where the phase velocity is able to exceed the speed of light. Known systems where effect takes place are the scattering of bosonic fields by rotating black holes, and the scattering of electromagnetic waves by a rotating cylinder made of electrical conductive material [13]. Superradiance is basically the transfer of energy from a given system to a wave scattering off this system. As such the scattered wave can have a larger amplitude than the incident one, "stealing" energy from the system it scatters off from. Because superradiance may take place in the background space-time of rotating black holes, one could suspect that a similar effect occurs in any rotating solution describing an acoustic black hole; because now we are discussing acoustic waves, we can refer to this as superresonance. Black holes can be made unstable against superradiance; e.g. if surrounded by a mirror (the back and forth bouncing of the waves at the reflecting wall and their subsequent amplification by superradiance close to the ergoregion are expected to turn the system into a BH bomb) [3, 4], or in a system with many black holes [27]. These instabilities are also expected to be found in acoustic black holes, and the ability to reproduce them in a laboratory could allow us to do further phenomenological exploration of high-energy physics, as well as to explore technology based in black hole physics.

In this chapter, we will show how this process occurs in an acoustic black hole and we will study the instabilities of acoustic black holes against superresonance in a system with many closely packed acoustic black holes.

4.1 Superradiance and superresonance

Let us consider a (massless) scalar field of the form $\psi\left(r,\theta,t\right)=\sqrt{r}H(r)e^{i(m\theta-\omega t)}$. Using equation (2.20) and the line element (2.33), the wave equation for this scalar field propagating in the fluid is

$$\partial_{\hat{\mathrm{r}}^*}^2 H+QH=0\,, \tag{4.1}$$

where

$$Q\equiv\left\{\left(\hat{\omega}-\frac{\hat{\mathrm{B}}m}{\hat{\mathrm{r}}^2}\right)^2-V\right\},\qquad V\equiv\left(\frac{\hat{r}^2-1}{\hat{r}^2}\right)\left[\frac{1}{\hat{r}^2}\left(m^2-\frac{1}{4}\right)+\frac{5}{4\hat{r}^4}\right], \tag{4.2}$$

where r_* is the *tortoise coordinate*, defined as (A.12). A full derivation of this wave equation can be found in Appendix A.

Close to the horizon, $r\to r_H$, and in the case of classical holes only (no Hawking radiation, no waves coming out of the black hole), we impose in-going waves only,

$$H\sim T_{\omega m}e^{-i(\omega-Bm)r_*}\qquad r\to r_H\,, \tag{4.3}$$

where $T_{\omega m}$ is the transmission coefficient. At infinity, where spacetime is flat, we set up an appropriate scattering experiment: an incident wave of unit amplitude and a reflected wave of amplitude $R_{\omega m}$,

$$H\sim e^{-i\omega r_*}+R_{\omega m}e^{+i\omega r_*}\qquad r\to\infty\,. \tag{4.4}$$

The above solution to the ordinary differential equation, with asymptotic behavior H_∞ and $H_{-\infty}$, is linearly independent from its complex conjugate. It is also easy to show that the wronskian $\mathcal{W}$ of two such solutions is a constant everywhere, for an wave equation of the form we are dealing with. As such, we get $\mathcal{W}(-\infty) = 2i(\omega - Bm)\left|T_{\omega m}\right|^2$ and $\mathcal{W}(\infty) = 2i\omega\left(1 - \left|R_{\omega m}\right|^2\right)$, which yields

$$\left|R_{\omega m}\right|^2 = 1 - \left(1 - \frac{Bm}{\omega}\right)\left|T_{\omega m}\right|^2 . \tag{4.5}$$

Therefore, superresonance ($\left|R_{\omega m}\right|^2 > 1$) will occur whenever the condition $\omega < Bm$ is satisfied.

The Vortex Geometry with constant density

We first discuss the geometry with constant background density. Hereafter, we set the horizon location at $r_H = 1$. In Figures 4.1-4.2 below, we show how the reflection coefficient $R_{\omega m}$ depends on the frequency ω, for different values of rotation B and azimuthal number m.

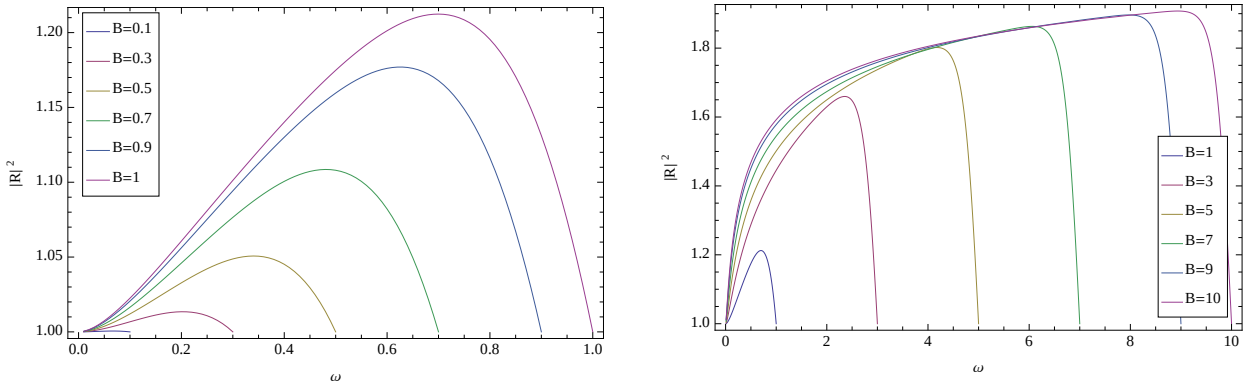

Figure 4.1: Superradiance for waves with $m = 1$, for different values of $B < 1$ (left panel) and $B > 1$ (right panel).

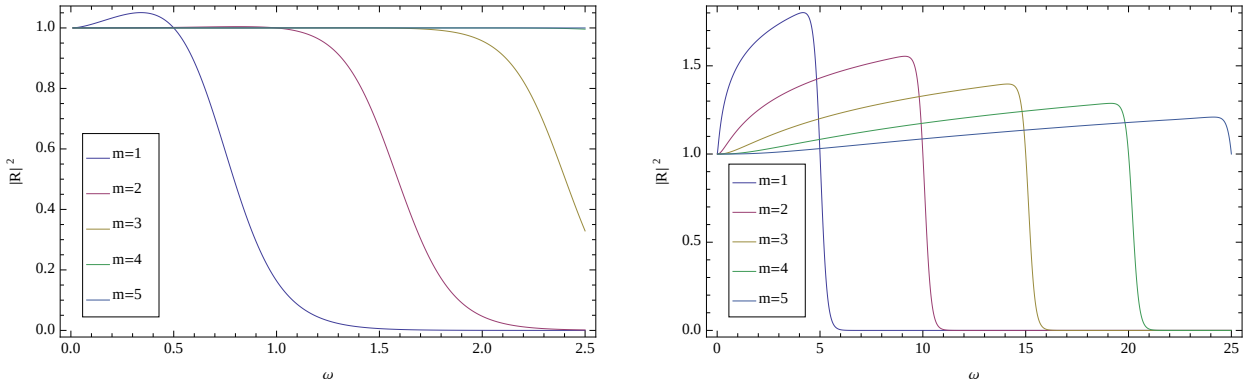

Figure 4.2: Superradiance for waves with different values of m, for values of $B = 0.5$ (left panel) and $B = 5$ (right panel).

Analyzing figure 4.2, we find that the maximum superresonant amplifications decreases as the azimuthal quantum number m increases. On the other hand, in figure 4.1 we find that the larger the rotation is,

the more amplified the reflected wave is. In table 4.1 we show the variation of the maximum reflection coefficient and the maximum frequency with B. Figure 4.3 is a plot of the variation of the maximum

Table 4.1: Variation of superresonant amplification with B, fixing $m = 1$

	B										
	1	5	10	15	20	25	30	35	40	45	50
$\lvert R\rvert^2_{max}$	1.212	1.802	1.907	1.941	1.956	1.966	1.972	1.977	1.98	1.984	1.988
ω_{max}	0.70	4.18	8.95	13.82	18.72	23.64	28.67	33.41	37.45	43.82	48.26

reflection coefficient with B; it becomes apparent that, for high values of B (*i.e.* $B \gtrsim 5$), the maximum superresonant amplification increases with $\frac{Log(B)}{B^{cte}}$. It can also be seen in table 4.1 that the frequency for which the maximum superresonant amplification occur increases in proportion with B.

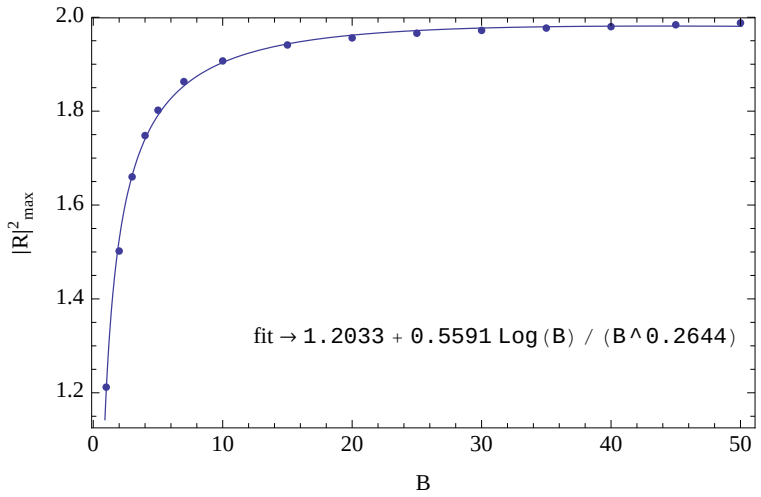

Figure 4.3: Variation of $|R|^2_{max}$ with B. The line is a fit for values between $B = 1$ and $B = 20$.

The Generalized Rotating Geometry

What happens for the non constant density case of (2.40)? Let's define the wave function as $\psi(r,\theta,t) = \frac{1}{\sqrt{c(r)r}}\Psi(r)e^{i(m\theta-\omega t)}$, then we have the wave function for $\Psi(r)$ given by the Schrodinger-like equation

$$\frac{d^2}{dr_*^2}\Psi(r) + \left(\frac{\left(\omega - mB/r^2\right)^2}{c(r)^2} - V\right)\Psi(r) = 0 \tag{4.6}$$

where we define r_* by $dr_*/dr = 1/f(r)$, and V is

$$V = \frac{f(r)}{4r^2c^2(r)}\left(-r^2f(r)(\partial_r c(r))^2 + c^2(r)\left(4m^2 - f(r) + 2r\partial_r f(r)\right) + 2rc(r)\partial_r(rf(r)\partial_r c(r))\right). \tag{4.7}$$

We will now specify that the speed of sound will follow a profile as in (2.41), $c = 2 - 1/r^n$. This generalization is going to be of major importance in the next section. In figure 4.4, we show the influence of the index n (found in equation (2.41)) in the potential (4.7), considering waves with azimuthal quantum number $m = 1$. Close to the horizon, the maximum in the potential is increasing in a quadratic way with the

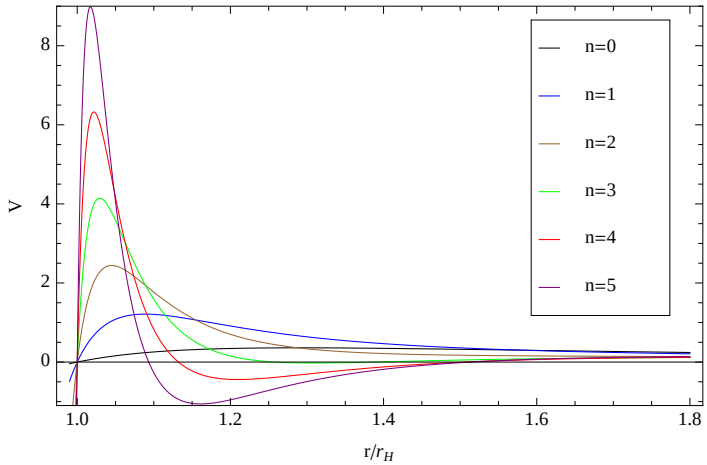

Figure 4.4: Influence of n in the potential

index n, while the radius at which the maximum occur varies in an inverse proportion with n. The maximum of the potential can be interpolated by the function

$$V_{max} = a_1 + b_1 n + c_1 n^2, \tag{4.8}$$

with

$$a_1 = 0.477836, \qquad b_1 = 0.501087, \qquad c_1 = 0.240035; \tag{4.9}$$

and the radius at wich the maximum occur can be interpolated by the function

$$r_{V_{max}} = a_2 + b_2 \frac{1}{n}, \tag{4.10}$$

with

$$a_2 = 0.999570, \qquad b_2 = 0.089335. \tag{4.11}$$

For $n \geqslant 3$, there's a region in figure 4.4 which becomes negative. Therefore, it is possible that the acoustic hole itself becomes unstable for those values of n, and if so, this might be a constraint for an experimental realization of an acoustic hole with the considered density profile. The minimum value of the potential (in the negative region) decreases quadratically with n and can be interpolated by the function

$$V_{min} = a_1' + b_1' n + c_1' n^2, \qquad n \geqslant 3, \tag{4.12}$$

$$a_1' = 0.270836, \qquad b_1' = -0.173379, \qquad c_1' = -0.091316; \tag{4.13}$$

and the radius at which the minimum occur can be interpolated by the function

$$r_{V_{min}} = a_2' + b_2' \frac{1}{n} + c_2' \frac{1}{n^2} + d_2' \frac{1}{n^3}, \qquad n \geqslant 3, \tag{4.14}$$

with

$$a_2' = 1.003699, \qquad b_2' = 0.646731, \qquad c_2' = -0.602953, \qquad d_2' = 0.261552. \tag{4.15}$$

In figure 4.5 we show a the plot of the amplification factor for different rotation B, for fixed $m = 1$ and $n = 10$.

Fixing $B = 5$ and $m = 1$, we can see in figure 4.6 that the bigger the n is, the bigger is the superradiance maximum, Comparing with the results in figure 4.1, we find that for $B = 1$ we have a smaller maximum of superresonant amplification then when considering a constant density ρ, for $B = 4$ we have a bigger maximum of superresonant amplification then in the case of constant ρ and for $B = 6$ we have a much bigger superresonant amplification then in the case of constant ρ.

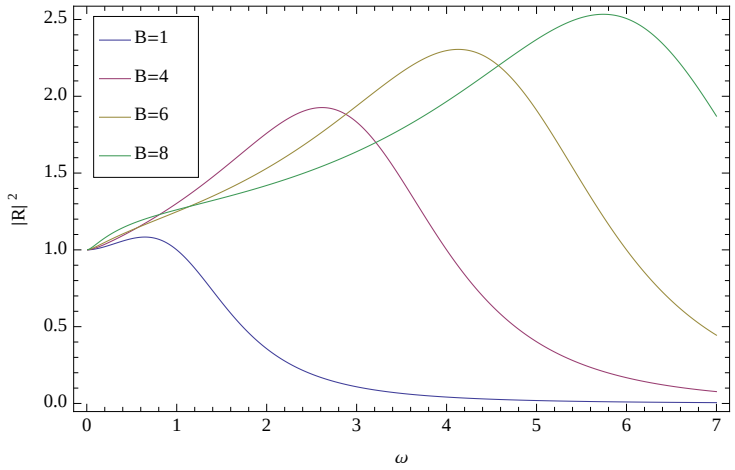

Figure 4.5: Superradiance with varying $c(r)$, fixing $m = 1$ and $n = 10$

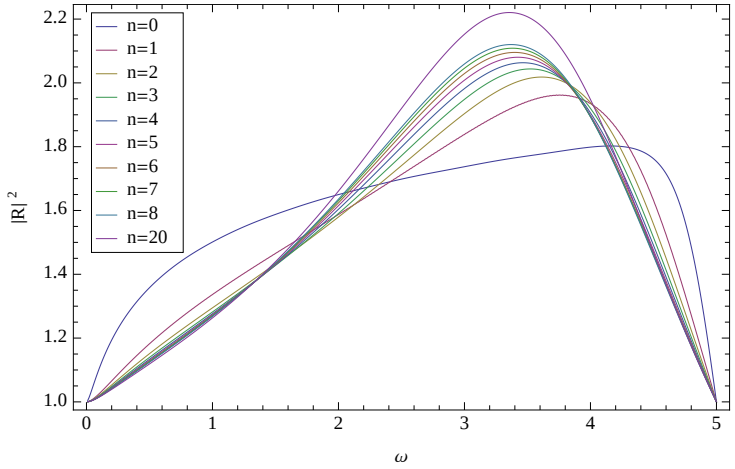

Figure 4.6: Superradiance with varying $c(r)$, fixing $m = 1$ and $B = 5$. The $n = 0$ is the case of constant ρ, and is found here for comparison

Figure 4.6 shows the variation of superresonant amplification with n, fixing $B = 5$ and $m = 1$. When $n = 0$ we return to the case of constant density. The maximum reflection coeficient $|R|^2_{max}$ increases slowly as n increases.

Figure 4.7, show several cases of superresonance for different values n and for $B = 8, 10$, considering $m = 1$.

In table 4.2 we show the variation of the maximum reflection coefficient and the maximum frequency with B, fixing $n = 5$ and the azimuthal mode $m = 1$, and figure 4.8 is a plot of the variation of the maximum reflection coefficient with B. Again, it becomes apparent that the maximum superresonant amplification increases with $\frac{Log(B)}{B^{cte}}$ when considering large values of B (*i.e.* $B \gtrsim 5$), and the frequency corresponding to the maximum superresonant amplification increases in proportion with B. As it can be seen in table 4.2, there is a limit for the maximum amount of energy that one can extract with this density profile, which occur at some value close to $B \sim 20.5$.

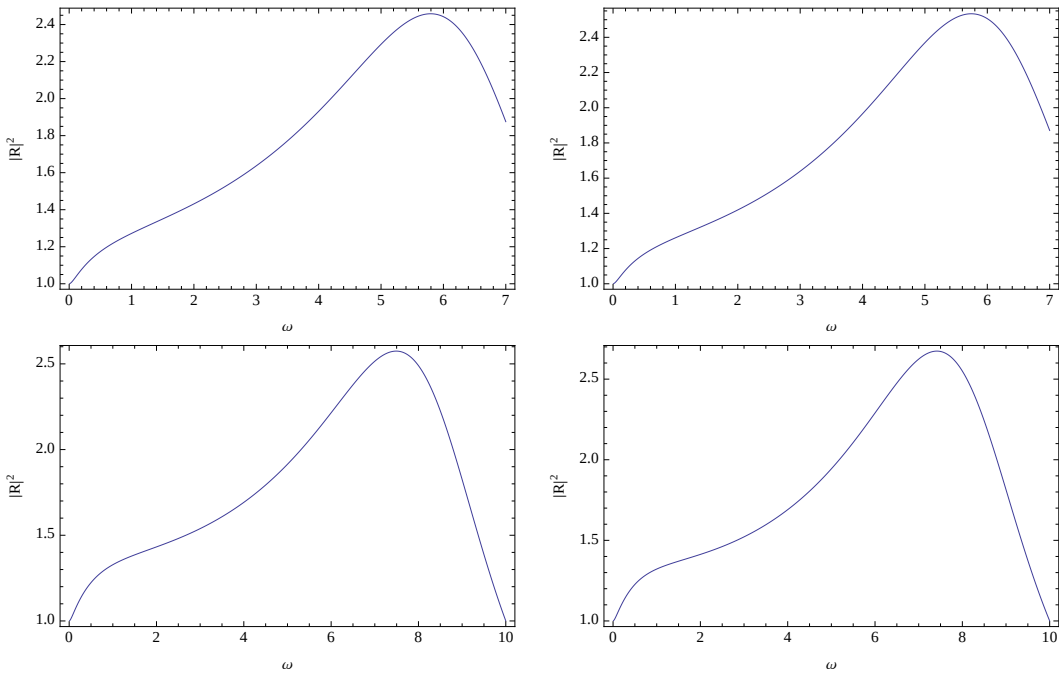

Figure 4.7: Superradiant amplification factors for varying sound velocity $c = 2 - 1/r^n$, and fixed $m = 1$, for different values of $B = 8, 10$ (top to bottom) and $n = 7, 10$ (left to right).

Table 4.2: Variation of superresonant amplification with B, fixing $m = 1$ and $n = 5$

	B											
	5	10	15	20	20.5	21	25	30	35	40	45	50
$\|R\|^2_{max}$	2.075	2.481	2.578	2.5968	2.5969	2.5968	2.591	2.576	2.558	2.54	2.521	2.504
ω_{max}	3.41	7.58	12.04	16.63	17.1	17.56	21.3	26.02	30.76	35.54	40.33	45.16

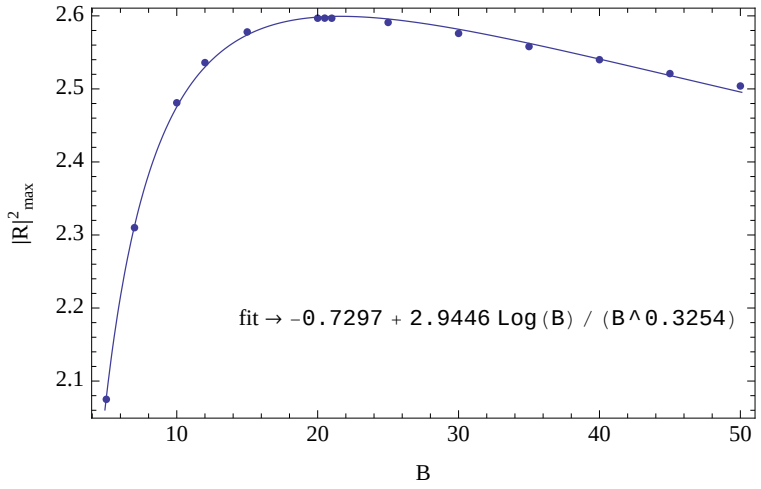

Figure 4.8: Variation of $|R|^2_{max}$ with B. The line is a fit for values between $B = 5$ and $B = 50$.

4.2 Superradiant Instabilities

We now want to search for superradiant instabilities. Let the absorption cross section for each mode m be defined as

$$\sigma_m = \frac{1}{\omega}(1 - |R|^2), \tag{4.16}$$

and for the total absorption cross section, we shall take the sum over all m's

$$\sigma = \sum_{m=-\infty}^{\infty} \frac{1}{\omega}(1 - |R|^2). \tag{4.17}$$

To find numerical solutions of (4.17), we will consider the sum for all $m's$ between $m \in [-20, 20]$. Furthermore, when considering co-rotating waves we will consider the sum in the interval $m \in [0, 20]$ and for counter-rotating waves we will consider the sum in the interval $m \in [-20, -1]$.

The Vortex Geometry with constant density

Exploring the absorption cross-section for the case of constant density ρ, we find always positive cross-sections, tending to a constant value at large frequencies. In figure 4.9 it's shown the numerical result for the total cross-section for waves entering in a non rotating fluid ($B = 0$). In figure 4.10 it's shown the numerical result

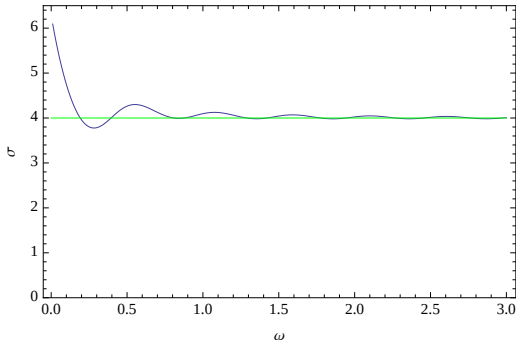

Figure 4.9: Total absorption cross-section for $B = 0$. The green line represents the expected cross-section in the high-frequency limit.

for the cross-section of co-rotating and counter-rotating waves entering in a fluid with $B = 1, 2, 3$. From our searches, the absorption cross-section seems to be always converging into some positive constant value, and therefore we don't find instabilities for the case of a fluid with constant density. These results seem to be in agreement with results found previously [29]. In table 4.3 we show the analytical results for the absorption cross-section obtained in chapter 3, and compare the sum of the analytical results for co-rotating and counter-rotating waves with the numerical sum for waves with positive and negative azimuthal modes m at large frequencies. We find that, in the high frequency limit, there seems to be a very good agreement

Table 4.3: Comparison of analytical and numerical results for the absorption cross-section

	B					
	0	1	2	3	4	5
co-rotating	2	0.828	0.472	0.325	0.246	0.198
counter-rotating	2	4.828	8.472	12.325	16.246	20.198
analytical sum	4	5.656	8.944	12.650	16.492	20.396
numerical sum	4	5.69	9.07	12.33	16.41	20.26

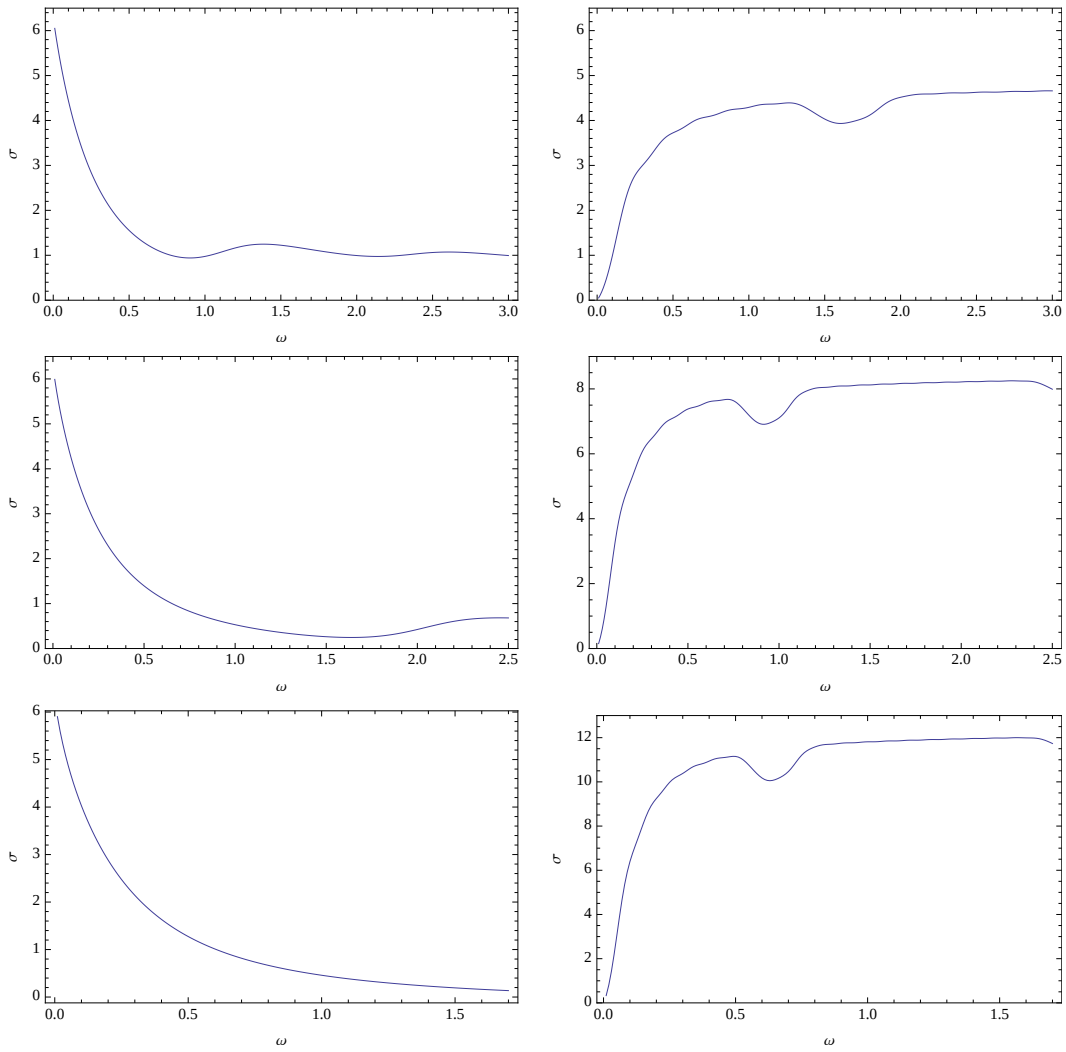

Figure 4.10: Absorption cross-section for $B = 1, 2, 3$ (top to bottom; left positive m, right negative m).

between the analytical and the numerical results. The results for $B = 0$ (figure 4.9) are in a remarkable excellent agreement.

The Generalized Rotating Geometry

The above analysis shows that, for constant density fluids, the absorption cross-section never seems to become negative. This was the reason which raised the motivation to generalize the *vortex geometry* to the case of varying density ρ. Considering now the wave equation (4.6), with the chosen profile for the speed of sound (2.41), we are now able to find negative values of the absorption cross-section if restricting our study for co-rotating modes. In figure 4.11, it is shown the absorption cross-section for $B = 5$ and different values of n, for co-rotating waves, in the case of non-constant density $\rho = c(r)$. Apparently, instabilities are found for frequencies ω close to the frequencies of the respective maximums of superradiant amplification with the mode $m = 1$. One can also see that, in the high frequency limit, the absorption cross-sections tend to the analytical results obtained in chapter 3. Figure 4.12 show the absorption cross-sections for $B = 8, 10$, summing over positive m's in the interval $m \in [0, 15]$. From our results it becomes apparent that the instabilities are always found around the frequencies of the maximum of superresonant amplification for the azimuthal mode

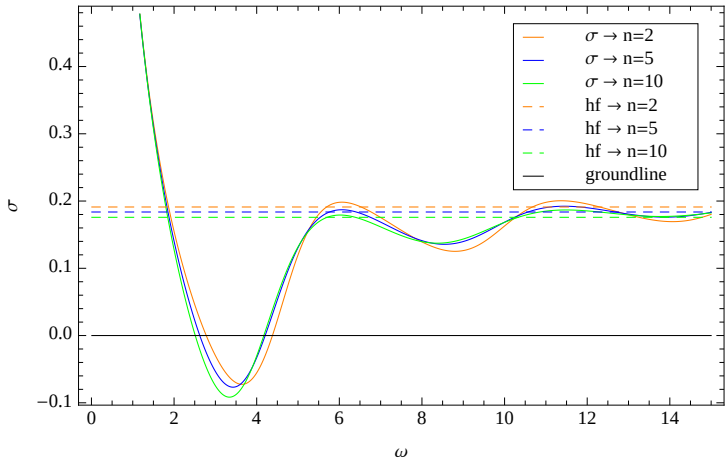

Figure 4.11: Absorption cross-section for $B = 5$ and various n's. In the legend, "σ" stands for the numerical result of the absorption cross-section and "hf" stands for high frequency limit.

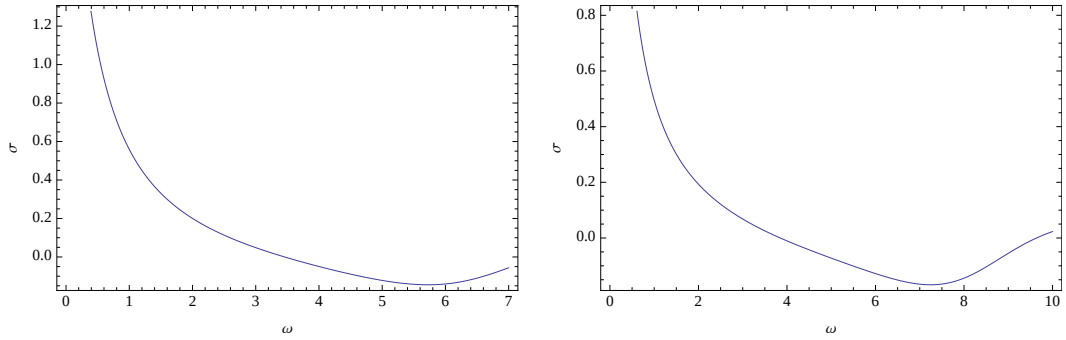

Figure 4.12: Absorption cross-section for $B = 8, n = 6$ and $B = 10, n = 10$.

$m = 1$ for each B, whenever $n \geqslant 1$. Of course that, since this instability occurs only for co-rotating modes, and not for the total sum of cross-sections for co- and counter-rotating waves, reproducing this phenomenon in laboratory conditions might be rather an hard task. However, from a classical point of view, knowing the sound waves angle of incidence on a first acoustic hole, one can determine the angle of reflection, and therefore, if one places a second acoustic hole in the way of the reflected sound wave, rotating in an opposite direction relatively to the direction of rotation of the first acoustic hole, and so on, it should in principle be possible to reproduce an experimental setup which would allow us to test this instability. This is an open question.

Chapter 5

Conclusions

The acoustic black hole is a powerful analogy to study experimentally general relativity, and in particular, to study experimentally some of the features of black holes physics. This analogy is well established and even more promising now that analogue black holes have been effectively implemented to measure Hawking-like radiation in the laboratory.

The main aim of this thesis was to study superradiance phenomena in acoustic black holes. We have reviewed the *"draining bathtub geometry"* assuming a constant density profile. This setting had already been explored in the literature, where it was found that superradiant mechanisms were not strong enough to de-stabilize the system. Here, we generalized this work in two directions: (i) by extending the geometry allowing the density to be non constant. (ii) we also considered many-body instabilities, in particular fission-like instabilities. We find it is possible to have a position-dependent density profile such that this instability occurs for certain frequencies *and* waves co-rotating with the acoustic black hole.

Acoustic black holes are not true black holes, because the acoustic metric satisfies the equations of fluid dynamics rather than Einstein's equations. One usually expresses this by saying that they are analogs *of* general relativity, because they provide an effective metric and so generate the basic kinematical background in which general relativity resides. They are not models *for* general relativity, because the metric is not dynamically dependent on something like Einstein's equations. However, analog geometries can be useful as constructions which can be implemented in the laboratory, and which display many features of Einsteinian black holes: classically, *any* process which depends only on background spacetime quantities can be mimicked in this way. For instance the geodesic structure describes propagation of high-frequency waves and even semi-classical effects such as Hawking radiation are shared by analogue geometries.

Appendix A

The Propagation of a Scalar Field in the Klein-Gordon Equation

Let's consider a massless scalar field ψ propagating in the (2+1) *"draining bathtub"* spacetime, such that $\psi = R(r)M(\theta)\tau(t)$. The Klein-Gordon equation gives the result

$$r^2(c^2r^2 - A^2)\frac{\partial_r^2 R(r)}{R(r)} - (B^2 - c^2r^2)\frac{\partial_\theta^2 M(\theta)}{M(\theta)} - r^4\frac{\partial_t^2\tau(t)}{\tau(t)} + r(A^2 + c^2r^2)\frac{\partial r R(r)}{R(r)} - 2AB\frac{\partial_\theta M(\theta)}{M(\theta)} +$$
$$+2ABr\frac{\partial_\theta M(\theta)}{M(\theta)}\frac{\partial r R(r)}{R(r)} - 2Br^2\frac{\partial_\theta M(\theta)}{M(\theta)}\frac{\partial_t\tau(t)}{\tau(t)} + 2Ar^3\frac{\partial_r R(r)}{R(r)}\frac{\partial_t\tau(t)}{\tau(t)} = 0\,. \tag{A.1}$$

Every angular function can be written as a Fourier series, so, we have $M(\theta) = \sum_m a_m e^{im\theta}$. Rewriting (A.1) placing $M(\theta)$ in evidence we have

$$\partial_\theta^2 M(\theta) + \beta(r,t)\partial_\theta M(\theta) + \Lambda(r,t)M(\theta) = 0, \tag{A.2}$$

with

$$\begin{aligned}\Lambda(r,t) &= -\left[r^2(c^2r^2 - A^2)\frac{\partial_r^2 R(r)}{R(r)} - r^4\frac{\partial_t^2\tau(t)}{\tau(t)} + r(A^2 + c^2r^2)\frac{\partial_r R(r)}{R(r)} + 2Ar^3\frac{\partial_r R(r)}{R(r)}\frac{\partial_t\tau(t)}{\tau(t)}\right]\left[B^2 - c^2r^2\right]^{-1}\\ \beta(r,t) &= \left[2AB\left(-r\frac{\partial_r R(r)}{R(r)} + \frac{r^2}{A}\frac{\partial_t\tau(t)}{\tau(t)} + 1\right)\right]\left[B^2 - c^2r^2\right]^{-1}\,.\end{aligned} \tag{A.3}$$

Replacing $M(\theta)$ with the Fourier series in (A.2) we find

$$\begin{aligned}&\sum_{m=-\infty}^{\infty}\left(-a_m m^2 e^{im\theta}\right) + \beta(r,t)\sum_{m=-\infty}^{\infty}\left(a_m ime^{im\theta}\right) + \Lambda(r,t)\sum_{m=-\infty}^{\infty}\left(a_m e^{im\theta}\right) = 0\\ \Leftrightarrow\quad &\sum_{m=-\infty}^{\infty}\left(-a_m m^2 e^{im\theta} + a_m ime^{im\theta}\beta(r,t) + a_m e^{im\theta}\Lambda(r,t)\right) = 0\\ \Leftrightarrow\quad &-m^2 + im\beta(r,t) + \Lambda(r,t) = 0\,,\end{aligned} \tag{A.4}$$

therefore, such an angular function behaves exactly like $M(\theta) = e^{im\theta}$. Every time functions can be written as a Fourier transform, and then we have $\tau(t) = \frac{1}{\sqrt{2\pi}}\int_{-\infty}^{\infty}\widehat{\tau}(\omega)e^{-i\omega t}d\omega$. In the same way we did for $M(\theta)$, we can rewrite now (A.1) as

$$\partial_t^2\tau(t) + \beta'(r,\theta)\partial_t\tau(t) + \Lambda'(r,\theta)\tau(t) = 0, \tag{A.5}$$

with the appropriate functions $\beta'(r,\theta)$ and $\Lambda'(r,\theta)$. Replacing the Fourier transform in (A.5) we find

$$\begin{aligned}
&\frac{1}{2\pi}\int_{-\infty}^{\infty}\left(-\widehat{\tau}(\omega)\omega^2 e^{-i\omega t}\right)d\omega+\frac{\beta'(r,\theta)}{2\pi}\int_{-\infty}^{\infty}\left(-\widehat{\tau}(\omega)i\omega e^{-i\omega t}\right)d\omega+\frac{\Lambda'(r,\theta)}{2\pi}\int_{-\infty}^{\infty}\left(\widehat{\tau}(\omega)e^{-i\omega t}\right)d\omega=0\\
\Leftrightarrow\quad&\frac{1}{2\pi}\int_{-\infty}^{\infty}\widehat{\tau}(\omega)\left(-\omega^2e^{-i\omega t}-i\omega e^{-i\omega t}\beta'(r,\theta)+e^{-i\omega t}\Lambda'(r,\theta)\right)d\omega=0\\
\Leftrightarrow\quad&-\omega^2-i\omega\beta'(r,\theta)+\Lambda'(r,\theta)=0\,,
\end{aligned}\tag{A.6}$$

and therefore, such a time function behaves exactly like $\tau(t)=e^{-i\omega t}$, so, our scalar field can be written as $\psi=R(r)e^{i(m\theta-\omega t)}$. Replacing this in equation (A.1) we get

$$\begin{aligned}
&2rABim\frac{\partial_r R(r)}{R(r)}-2Br^2m\omega-2ABim+m^2(B^2-c^2r^2)-2Ar^3i\omega\frac{\partial_r R(r)}{R(r)}+(A^2+c^2r^2)r\frac{\partial_r R(r)}{R(r)}+\\
&+(c^2r^2-A^2)r^2\frac{\partial_r^2R(r)}{R(r)}+r^4\omega^2=\\
=\quad&\partial_r^2R(r)+\frac{A^2+c^2r^2+2iA\left(Bm-r^2\omega\right)}{r\left(c^2r^2-A^2\right)}\partial_rR(r)+\frac{r^4\omega^2-2Br^2m\omega-2ABim+m^2\left(B^2-c^2r^2\right)}{r^2\left(c^2r^2-A^2\right)}R(r)=\\
=\quad&0\,,
\end{aligned}\tag{A.7}$$

which we will rewrite as

$$\partial_r^2R(r)+P_1\partial_rR(r)+Q_1R(r)=0,\tag{A.8}$$

with

$$P_1=\frac{A^2+c^2r^2+2iA\left(Bm-r^2\omega\right)}{r\left(c^2r^2-A^2\right)},\tag{A.9}$$

$$Q_1=\frac{r^4\omega^2-2Br^2m\omega-2ABim+m^2\left(B^2-c^2r^2\right)}{r^2\left(c^2r^2-A^2\right)}\,.\tag{A.10}$$

It would be interesting to study this wave function in $]-\infty,\infty[$, however, the coordinate r is defined in $r\in[0,\infty[$. Let us now introduce the *tortoise coordinate* r_*. This coordinate r_* shall be such that whenever $r=r_H$, we have $r_*=-\infty$, and whenever $r=\infty$ we have $r_*=\infty$, and therefore we will have $r_*\in]-\infty,\infty[$. Considering the g_{rr} term in 2.33, which in fact is $-\infty$ when $r=r_H$, let us define the *tortoise coordinate* by

$$\frac{dr_*}{dr}=\Delta\equiv\left(1-\frac{A^2}{c^2r^2}\right)^{-1},\tag{A.11}$$

so

$$r_*=r+\frac{A}{2c}log\left|\frac{cr-A}{cr+A}\right|.\tag{A.12}$$

Substituting $R(r)=Z(r)H(r_*)$, we'll find (A.8) to be

$$\begin{aligned}
&\partial_r^2(ZH)+P_1\partial_r(ZH)+Q_1ZH=\\
=\quad&\partial_r(H\partial_rZ+Z\partial_rr_*\partial_{r_*}H)+P_1H\partial_rZ+P_1Z\partial_rr_*\partial_{r_*}H+Q_1ZH=\\
=\quad&H\partial_r^2Z+2\Delta\partial_{r_*}H\partial_rZ+Z\Delta^2\partial_{r_*}^2H+Z\partial_{r_*}H\partial_r\Delta+P_1Z\Delta\partial_{r_*}H+P_1H\partial_rZ+Q_1ZH=\\
=\quad&Z\Delta^2\partial_{r_*}^2H+[\Delta(2\partial_rZ+P_1Z)+\Delta^{'}Z]\partial_{r_*}H+(\partial_r^2Z+P_1\partial_rZ+Q_1Z)H=0\,.
\end{aligned}\tag{A.13}$$

We know want to impose that the coefficient $\partial_{r_*}H$ be null. Therefore

$$\begin{aligned}
&\Delta(2\partial_rZ+P_1Z)+\Delta^{'}Z=0\\
\Leftrightarrow\quad&\partial_rZ+\left(\frac{P_1}{2}+\frac{\Delta^{'}}{2\Delta}\right)Z=0\\
\Leftrightarrow\quad&\partial_rZ+\left(\frac{P_1}{2}-\frac{A^2}{r(c^2r^2-A^2)}\right)Z=0\\
\Leftrightarrow\quad&\partial_rZ+\left(\frac{-A^2+r^2c^2+2iA(Bm-r^2\omega)}{2r(r^2c^2-A^2)}\right)Z=0\,.
\end{aligned}\tag{A.14}$$

Solving equation (A.14), one finds

$$Z(r) = Z_k e^{-\int \frac{-A^2+r^2c^2+2iA(Bm-r^2\omega)}{2r(r^2c^2-A^2)}dr}, \tag{A.15}$$

and the integral yields

$$-\int \frac{-A^2+r^2c^2+2iA(Bm-r^2\omega)}{2r(r^2c^2-A^2)}dr = \frac{(-A+2iBm)\mathrm{Log}(r)}{2A} + \frac{i\left(-Bc^2m+A^2\omega\right)\mathrm{Log}\left(-A^2+c^2r^2\right)}{2Ac^2}, \tag{A.16}$$

therefore,

$$Z(r) = Z_k\ exp\left[\left(\frac{iBm}{A}-\frac{1}{2}\right)\mathrm{Log}(r) + \frac{i\left(-Bc^2m+A^2\omega\right)\mathrm{Log}(-A^2+c^2r^2)}{2Ac^2}\right]. \tag{A.17}$$

this result can be rewritten as

$$\begin{aligned} Z(r) &= Z_k\ exp\left[\left(\frac{iBm}{A}-\frac{1}{2}-\frac{1}{2}+\frac{1}{2}\right)\mathrm{Log}(r) + \frac{i\left(-Bc^2m+A^2\omega\right)\mathrm{Log}(-A^2+c^2r^2)}{2Ac^2}\right] = \\ &= \sqrt{r}\ Z_k\ exp\left[\left(\frac{iBm}{A}-1\right)\mathrm{Log}(r) + \frac{i\left(-Bc^2m+A^2\omega\right)\mathrm{Log}(-A^2+c^2r^2)}{2Ac^2}\right]. \end{aligned} \tag{A.18}$$

Replacing the solution (A.18) in (A.13), we find

$$\begin{aligned} &\partial^2_{r_*}H + \frac{1}{\Delta^2}\left(\frac{\partial^2_r Z}{Z} + P_1\frac{\partial_r Z}{Z} + Q_1\right)H = \\ &\partial^2_{r_*}H + \left[\frac{5}{4}\frac{A^4}{c^4r^6} + \frac{A^2\left(m^2-\frac{3}{2}\right)+B^2m^2}{c^2r^4} - \frac{2Bm\frac{\omega}{c^2}-\frac{1}{4}+m^2}{r^2} + \frac{\omega^2}{c^2}\right]H = 0\,. \end{aligned} \tag{A.19}$$

Rescaling units so that we have the horizon radius $r_H = 1$, having then $A = c = 1$, we can rewrite equation (A.19) as

$$\partial^2_{\hat{\mathrm{r}}^*}H + QH = 0, \tag{A.20}$$

where

$$Q \equiv \left\{\left(\hat{\omega} - \frac{\hat{\mathrm{B}}m}{\hat{\mathrm{r}}^2}\right)^2 - V\right\}, \quad V \equiv \left(\frac{\hat{r}^2-1}{\hat{r}^2}\right)\left[\frac{1}{\hat{r}^2}\left(m^2-\frac{1}{4}\right)+\frac{5}{4\hat{r}^4}\right]. \tag{A.21}$$

Bibliography

[1] W. G. Unruh, *Experimental Black-Hole Evaporation?*, Phys.Rev.Lett. 46, 21 (1981)

[2] M. Visser, *Acoustic black holes: horizons, ergospheres, and Hawking radiation*, arxiv: gr-qc/9712010 (1997)

[3] E. Berti, V. Cardoso, J. P. S. Lemos, *Quasinormal modes and classical wave propagation in analogue black holes*, Phys.Rev. D 70, 124006, arxiv: gr-qc/0408099v2 (2004)

[4] V. Cardoso, J. P. S. Lemos, S. Yoshida, *Quasinormal modes and stability of the rotating acoustic black hole: numerical analysis*, Phys.Rev D 70, 124032, arxiv: gr-qc/0410107v2 (2004)

[5] S. Chandrasekhar, *The Mathematical Theory of Black Holes*, Oxford University Press (1983)

[6] C. Misner, K. Thorne, J. Wheeler, *Gravitation*, W. Freeman and Company (1973)

[7] S.W. Hawking, *Particle creation by black holes*, Commun. Math. Phys. 43 199-220 (1975)

[8] M. Visser, *Acoustic propagation in fluids: an unexpected example of Lorentzian geometry*, arxiv:gr-qc/9311028 (1993)

[9] U. R. Fischer, R. Schutzhold, *Quantum simulation of cosmic inflation in two component Bose-Einstein condensates*, Phys.Rev.A 70, 063615 (2004)

[10] C. Barceló, S. Liberati, M. Visser, *Analogue gravity* arxiv: gr-qc/0505065 (2005)

[11] S. Weinfurtner, E. W. Tedford, M. C. J. Penrice, W. G. Unruh, G. A. Lawrence, *Measurement of stimulated Hawking emission in an analogue system*, arxiv: gr-qc/1008.1911 (2010)

[12] F. Belgiorno, S. L. Cacciatori, M. Clerici, V. Gorini, G. Ortenzi, L. Rizzi, E. Rubino, V. G. Sala, D. Faccio, *Hawking radiation from ultra short laser pulse filaments*, arxiv: gr-qc/1009.4634 (2010)

[13] M. Richartz, S. Weinfurtner, A. J. Penner, W. G. Unruh, *General univeral superradiant scattering*, Phys.Rev. D 80, 124016, arxiv: gr-qc/0909.2317 (2009)

[14] O. Lahav, A. Itah, A. Blumkin, C. Gordon, J. Steinhauer, *A sonic black hole in a density-inverted Bose-Einstein condensate*, arxiv: 0906.1337 (2009)

[15] L. J. Garay, J. R. Anglin, J. I. Cirac, P. Zoller, *Sonic black holes in dilute Bose-Einstein condensates*, Phys.Rev. A 63, 023611, arxiv: gr-qc/0005131 (2001)

[16] Y. Nambu, H. Iwayama, H. Saida, T. Shoji, *Acoustic Black Hole in Plasma Flow-Theory: Observation of a Classical Analogue to the Hawking Radiation*, J. Plasma Fusion Res. SERIES, Vol.8 (2009)

[17] C. Barceló, L. J. Garay, G. Janes, *The two faces of quantum sound*, Phys. Rev. D 82, 044042 arxiv: gr-qc/1006.0181(2010)

[18] R. Schutzhold, *Recreating Fundamental Effects in the Laboratory?*, arxiv: gr-qc/1004.2394

[19] P. D. Nation, M. P. Blencowe, A. J. Rimberg, E. Buks, *Analogue Hawking Radiation in a dc-SQUID Array Transmission Line*, Phys.Rev. Letters 103, 087004 (2009)

[20] B. Horstmann, B. Reznik, S. Fagnocchi, J. I. Cirac, *Hawking Radiation from an Acoustic Black Hole on an Ion Ring*, Phys.Rev.Letters 104, 250403 arxiv: quant-ph/0904.4801(2010)

[21] F. Federici, C. Cherubini, S. Succi, M. P. Tosi, *Superradiance from BEC vortices: a numerical study*, Phys.Rev. A 73, 033604 arxiv: gr-qc/0503089 (2006)

[22] S. Finazzi, R. Parentani, *Black hole laser in Bose-Einstein condensates*, New J. Phys. 12 095015, arxiv: cond-mat/1005.4024 (2010)

[23] A. Coutant, R. Parentani, *Black hole lasers, a mode analysis*, Phys.Rev. D 81, 084042 arxiv: hep-th/0912.2755 (2010)

[24] S. Fagnocchi, *Back-reaction in acoustic black holes*, J. Phys. Conference Series 33 arXiv: gr-qc/0601084 (2006)

[25] I. Carusotto, S. Fagnocchi, A. Recati, R. Balbinot, A. Fabbri, *Numerical observation of Hawking radiation from acoustic black holes in atomic Bose-Einstein condensates*, New J. Phys. 10, arXiv: 0803.0507 (2008)

[26] S. A. Teukolsky, W. H. Press, *Perturbations Of A Rotating Black Hole. III . Interaction Of The Hole With Gravitational And Electromagnetic Radiation*, Astrophys. J. 193, 443 (1974)

[27] W. H. Press and S. A. Teukolsky, *Floating Orbits, Superradiant Scattering and Black-hole Bomb*, Nature 238, 211 (1972)

[28] U. Leonhardt and P. Piwnicki, *Relativistic Effects of Light in Moving Media with Extremely Low Group Velocity*, Phys. Rev. Lett. 84, 5, (2000)

[29] E. S. Oliveira, S. R. Dolan, L. C. B. Crispino, *Absorption of planar waves in a draining bathtub*, Phys. Rev. D 81, 124013 (2010)